On the regional-scale variability of flow duration curves in Peninsular India

Pankaj Dey[1], Jeenu Mathai[2], Murugesu Sivapalan[3,4] and Pradeep. P. Mujumdar[5,6]

[1]Department of Hydrology, Indian Institute of Technology, Roorkee, India

[2]Marine Geoscience Group, National Centre for Earth Science Studies, Thiruvananthapuram, India

[3]Department of Civil and Environmental Engineering, University of Illinois at Urbana-Champaign, Urbana, IL, USA

[4]Department of Geography and Geographic Information Science, University of Illinois at Urbana-Champaign, Urbana, IL, USA

[5]Department of Civil Engineering, Indian Institute of Science, Bangalore, India

[6]Interdisciplinary Centre for Water Research, Indian Institute of Science, Bangalore, India

Correspondence to: Pankaj Dey (pdey609@gmail.com)

Abstract. As each catchment responds uniquely, even when appearing similar, formulating generalizable hypotheses and using routinely employed signatures of catchment similarity to examine streamflow variability can be challenging. The Flow Duration Curve (FDC), offering a concise portrayal of streamflow variability at a specific gauging station, provides insights into hydroclimatic and landscape processes operating across a broad range of spatial and temporal scales that govern flow regimes in a region. This study delves into the controls of streamflow variability in Peninsular India, specifically focusing on low-gradient rivers flowing east from the Western Ghats. The novelty of the study lies in partitioning streamflow into three time-wise categories (non-monsoon, southwest monsoon, northeast monsoon) and two process-related partitions (fast flow and slow flow) using FDCs. The methodology enables a detailed examination of the contributions of each season and process to the overall annual flow. The study further enhances its novelty by accompanying an in-depth analysis of FDCs, incorporating a Mixed Gamma Distribution (MGD) to model both fast and slow flow components. Uncovering the influence of climate, geology, and hydrological processes on MGD parameters, the study provides an advanced understanding of flow duration curve shapes. A key advancement is the integration of a comprehensive analysis of time scale decomposition, process decomposition, and statistical analyses, offering an in-depth exploration of streamflow variability controls in Peninsular India, contributing significantly to advancing our understanding of the complex interactions shaping streamflow patterns in the region.

1 Introduction

The hydrologic functioning of catchment systems in any given region is coevolved with the long-term climatology and landscape features present in the region through mutual interactions operating across multiple spatial and temporal scales (Wagener et al., 2013). These interactions and long-term feedbacks impart variability to hydrologic processes that are characteristic of the region of interest, including runoff generation and riverine transport processes, thus influencing water availability and reliability to human populations that depend on the streamflow. Understanding streamflow variability in time and space across river basins in the region is therefore

38 very important for water resource management (Deshpande et al., 2016; Sinha et al., 2018) and the prediction and

39 mitigation of floods (Kale et al., 1997). The frequency of high flows, low flows, or flows within specific ranges,

40 is essential for risk assessment of water management projects involving control of streamflow variability. Correct

41 portrayal of streamflow variability at the scale of catchments and river basins is therefore an indispensable

42 component in many hydrologic applications.

43 The focus of this paper is on the flow duration curve (FDC), which is a compact description of temporal

44 streamflow variability at the catchment scale. The FDC represents (daily) streamflow values plotted against the

45 proportion of time the given flow is exceeded or equalled (Smakhtin, 2001; Vogel & Fennessey, 1994). The

46 graphical form of the FDC embeds the governing hydrologic processes and dominant flow characteristics

47 throughout the range of recorded streamflow at the catchment scale (Botter et al., 2008). In this sense, the FDC is

48 also an important signature of a catchment's rainfall to runoff transformation (Ghotbi et al., 2020a; Vogel &

49 Fennessey, 1994). FDC thus typifies the old proverb, "one picture is worth a thousand words" with its potential

50 to encapsulate much of the relevant information of streamflow variability in a single plot (Vogel & Fennessey,

51 1995), and has been used in many hydrologic applications. Vogel and Fennessey (1994) provide a brief history of

52 the application of flow duration curves in hydrology. Applications of FDC include waste load allocation (Searcy,

53 1959), water quality management (Searcy, 1959; Rehana & Mujumdar, 2011, 2012), reservoir and sedimentation

54 studies (Vogel & Fennessey, 1995), low-flow and flood analyses (Smakhtin, 2001), assessment of environmental

55 flow requirements (Smakhtin and Anputhas, 2006), and water availability for hydropower (Basso & Botter, 2012).

56 Streamflow observed in rivers results from the complex interplay of various hydrological processes, including

57 runoff generation, overland and subsurface flow, and evaporation. These processes operate across multiple time

58 and space scales, responding to climatic inputs and interacting with heterogeneous landscape properties.

59 Deciphering the controls on streamflow variability and understanding their manifestation in the FDC shape pose

60 significant challenges (Cheng et al., 2012; Ghotbi et al., 2020b; Yokoo & Sivapalan, 2011). Therefore, identifying

61 the process controls is essential to develop appropriate conceptual frameworks. This approach enables the

62 generation of profound insights into the governing principles that underpin the observed variability in catchments.

63 To address this complexity, Yokoo and Sivapalan (2011) proposed a conceptual framework for unravelling the

64 process controls of the FDC. They considered the Total Flow Duration Curve (TFDC) as a statistical summation

65 of a Fast Flow Duration Curve (FFDC) and a Slow Flow Duration Curve (SFDC). The FFDC, representing a

66 filtered version of precipitation variability, is influenced by rainfall intensity patterns and surface soil

67 characteristics. In contrast, the SFDC reflects the competition between subsurface drainage and

68 evapotranspiration, with seasonality and regional geology playing stronger roles (Yokoo & Sivapalan, 2011). This

69 distinction between fast (surface runoff) and slow (subsurface streamflow and groundwater flow) flow time scales

70 allows for a nuanced understanding of the process controls governing each component separately (Cheng et al.,

71 2012; Yokoo & Sivapalan, 2011).

72 Ghotbi et al (2020a, 2020b) used this framework to explore the climatic and landscape controls of FDCs using

73 streamflow data for hundreds of catchments across the continental United States in a comparative manner. In

74 their work Ghotbi et al. (2020a) emphasized the need to consider the fast flow and slow flow time series

75 independently as stochastic responses of catchments to sequences of storm events. Intensity and frequency of

76 rainfall events and the properties of soils and topography govern the variability of fast flows, whereas climate
77 seasonality and regional geology of the aquifer system govern variability of slow flow components. More
78 specifically, Ghotbi et al. (2020b) showed the dominant process controls of FDCs as aridity index, topographic
79 slope, coefficient of variation of daily precipitation, timing of rainfall, time interval between storms, snow fraction,
80 and recession slope.

81 Stewart (2015) introduces the Bump and Rise Method (BRM), a novel baseflow separation technique calibrated
82 with tracer data or optimization methods for accurate replication of tracer-determined baseflow shapes. The study
83 challenges the conventional practice of solely relying on streamflow for recession analysis, contending that it can
84 be misleading in understanding catchment storage reservoirs. The study also suggests for implementing baseflow
85 separation before recession analysis as a means to gain fresh insights into water storage reservoirs and potentially
86 resolve existing issues associated with recession analysis.

87 Significant advancements have been achieved in unravelling the process controls influencing flow duration
88 curves. However, challenges persist in extending this knowledge to large spatial scales. To address this, Leong
89 and Yokoo (2022) proposed an innovative approach, aiming to enhance the flexibility and adaptability of
90 hydrological models by transforming the representation of the subsurface component. This involves the creation
91 of a flexible structure composed of interconnected linear reservoirs, derived from a distinctive multiple
92 hydrograph separation procedure, offering a comprehensive interpretation of dominant processes impacting FDC
93 shapes and understand the number of distinct hydrological processes involved. In this study, we adopted the
94 method proposed by Ghotbi et al. (2020) and (2021) as a foundational step to characterize fast and slow flow
95 components, recognizing its inherent limitations stemming from its empirical and subjective nature.

96 Botter et al. (2008) addressed river basin streamflow variability by presenting a seasonal probability distribution
97 for daily streamflow using a stochastic soil moisture model. Extending this to the annual scale, the study
98 establishes analytical expressions for long-term flow duration curves, linking them to annual minima distribution
99 through key basin parameters, including climate, ecohydrology, and geomorphology. Muller et al. (2014) presents
100 a process-based analytical expression for flow duration curves in seasonally dry climates, employing a stochastic
101 model for wet season streamflow and a deterministic recession with stochastic initial conditions for the dry season.
102 The approach disentangles inter- and intra-annual streamflow variations effectively. Durighetto et al. (2022)
103 develops analytical expressions for flow duration curves and stream length duration curves (SLDC) to classify
104 streamflow and active length regimes in temporary rivers. It identifies two streamflow regimes (persistent and
105 erratic) and three active length regimes (ephemeral, perennial, and ephemeral de facto) based on dimensionless
106 parameters linked to streamflow fluctuations and catchment discharge sensitivity. The proposed framework,
107 validated in Italy and USA catchments, reveals a structural relationship between streamflow and active length
108 regimes, offering a promising tool for analysing discharge and river network length dynamics in temporary
109 streams.

110 Our approach to understanding spatial patterns across Peninsular India builds upon the foundational concept of
111 timescale decomposition, as previously explored in studies such as Botter et al. (2008), Muller et al. (2014), and
112 Durighetto et al. (2022). The decomposition of timescales, while not novel in our study, serves as a fundamental
113 framework, aiding our analysis of spatial dynamics in the region.

114 The novelty of the paper lies in exploring the controls of streamflow variability in Peninsular India, a result of the
115 impacts of monsoons – southwest (summer season) and northeast (winter season), the presence of western and
116 eastern ghats, and topographical gradients. The paper advances the field by partitioning streamflow into three
117 distinct time-wise categories (non-monsoon, southwest monsoon, and northeast monsoon) and two process-wise
118 partitions (fast flow and slow flow), using flow duration curves as a tool. This approach allows for a detailed
119 examination of the relative contributions of each season and process to the overall annual flow.

120 Furthermore, the integration of a comprehensive approach to analysing flow duration curves by incorporating a
121 Mixed Gamma Distribution (MGD) to model both fast and slow flow components, along with seasonal and
122 regional exploration, enhances the study's novelty, and the study uncovers the influence of climate, geology, and
123 hydrological processes on MGD parameters, providing a better understanding of flow duration curve shapes. The
124 inclusion of links between MGD parameters and landscape properties, as well as the association between the
125 midsection slope of the FDC and recession parameters, adds an additional layer of sophistication to the analysis.
126 This provides a more robust understanding and offers insights into spatial variations, highlighting the integrated
127 role of surface and subsurface processes in shaping the catchment's average flow regime

128 The study stands out for its innovative combination of time scale decomposition, process decomposition, and
129 statistical analyses, offering a holistic exploration of the controls of streamflow variability in Peninsular India.
130 The partitioning approach and the integration of statistical analysis contribute significantly to advancing our
131 understanding of the complex interactions shaping streamflow patterns in this region. We recognize the abundance
132 of literature in FDC studies, but we believe our contribution is valuable in providing a detailed understanding of
133 the controls on streamflow variability in the context of Peninsular India.

134 Leong and Yokoo (2022) introduced an innovative approach, employing interconnected linear reservoirs to
135 enhance hydrological model flexibility and adaptability. Carlier et al. (2018) addressed the neglect of geological
136 characteristics in catchment studies, revealing that climate conditions predominantly influence medium to high
137 discharge percentiles, while the catchment's ability to buffer meteorological forcing is attributed to geological
138 features. Botter et al. (2013) identified an index incorporating climate and landscape attributes to discriminate
139 between erratic and persistent flow regimes, providing a robust framework for characterizing hydrology in the
140 face of global change. Basso et al. (2015) investigated the role of non-linear storage–discharge relations in shaping
141 high-flow distributions, emphasizing the importance of analysing individual events for accurate characterization.
142 Ye et al. (2012) explored regional variations in streamflow regime behaviour across the U.S., highlighting the
143 significance of snowmelt, vegetation cover dynamics, and climate trends. Fenicia et al. (2014) linked perceptual
144 hydrological models with mathematical structures, demonstrating how distinct catchment processes influence
145 model performance and emphasizing the need to synthesize experimentalist and modeler perspectives. Together,
146 these studies contribute to a comprehensive understanding of FDCs and advance our knowledge of hydrological
147 processes at different scales.

148 While the existing literature, represented by studies such as Leong and Yokoo (2022), Carlier et al. (2018), Botter
149 et al. (2013), Basso et al. (2015), Ye et al. (2012), and Fenicia et al. (2014), has made significant strides in
150 understanding the controls of flow duration curves and streamflow variability, our study distinguishes itself by
151 focusing on the unique hydrological context of Peninsular India. The previously discussed works have primarily

addressed FDC drivers at regional or global scales, examining factors such as hydrogeology, climate, and landscape alterations. In contrast, our study delves into the specific challenges posed by the Peninsular Indian environment, characterized by the interplay of monsoons, mountainous terrain, and topographical gradients. Through a comprehensive approach encompassing time scale decomposition and process decomposition, and statistical analyses, we employ FDC as a key tool to unravel the controls of streamflow variability across Peninsular India. Our work enhances the understanding of hydrological processes in a region with distinct monsoonal influences, thus advancing the state of the art and providing valuable insights for water resource management in Peninsular India.

The remainder of the paper is structured as follows. Section 2 elaborates on the details of the study area and the daily streamflow dataset used. The description of the methodology employed for the analysis is presented in Section 3. The results of the application of the framework to Peninsular India and the interpretation of the results are presented in Sections 4 and 5, respectively. Finally, the paper is concluded in Section 6 with key insights gained for the nature and controls of streamflow variability across Peninsular India.

2 Study region

Peninsular India is a cratonic region with an approximate shape of a vast inverted triangle with diverse topography and characteristic climatic patterns, bounded by the Arabian Sea in the west, the Bay of Bengal in the east, and the Vindhya and Satpura ranges in the north. The long escarpments of the Western Ghats and the Eastern Ghats, constituting the western and eastern continental fringes of India, and an asymmetric relief with eastward tilt towards the floodplains of several eastward draining rivers from the 1.5 km high Western Ghats, characterize the physiography of Peninsular India (Richards et al., 2016). The rise of the Himalayan-Tibetan plateau has significantly contributed to the Neogene climate of Asia, favoured the birth of the modern monsoon (Fig. 1.a, b) (Chatterjee et al., 2013, 2017), and triggered glaciation in the Northern region. A wide variety of plateaux, open valleys, bedrock gorges, mountain ranges, inselbergs and residual hills constitute the geomorphology of Peninsular India (Kale & Vaidyanadhan, 2014). The Peninsular landscape is dominated by Deccan Traps (Deccan basalts) of Cretaceous-Eocene, igneous and metamorphic rocks (Granite-gneisses) of Archaean-Late Precambrian along with minor consolidated sediments (Sandstone, shale) of Precambrian-Jurassic (Fig. 1.c) (Kale, 2014).

The region is strongly impacted by monsoons, major seasonal winds which are a manifestation of the seasonal movement of the Intertropical Convergence Zone (ICTZ in Fig. 1.a and Fig. 1.b), which contribute largely to the annual rainfall variability in much of the Indian subcontinent (Gadgil, 2003). The monsoons have two components – South-West monsoon and North-East monsoon, which arrive during June – September (JJAS) and October – December (OND), respectively. South-West monsoon season contributes more than 75% of annual rainfall over majority of the regions of the country (Saha et al., 1979). However, the Southern Peninsula receives a significant portion (30-60%) of its annual rainfall during the North-East monsoon, which contributes only 11% of the rainfall annually to India as a whole (Rajeevan et al., 2012). The maximum extent of rainfall over the Southern Peninsula during the North-East Monsoon is due to the reversal of lower-level winds over South Asia from the South-West to the North-East during the retreating phase of the South-West monsoon (Rajeevan et al., 2012). Peninsular India displays south-to-north variability in the South-West monsoon, causing heavy rainfall along the Western Ghats and reduced amounts in the central and northeastern regions (Fig S2.a in Supplementary Material).

190   The Western Ghats' long escarpment hosts predominantly tropical evergreen forest, crucial for intercepting South-
191   West monsoon winds (Ramachandra, 2018). Ramachandra (2018) depicted a west-east vegetation gradient along
192   the Western Ghats, transitioning from tropical-evergreen to semi-evergreen and progressing to moist to dry
193   deciduous forests towards the rain-shadow region in the east. The topography map for the Peninsular region and
194   a selected point in the region is depicted in Fig. S1.a and Fig. S1.b in Supplementary Material, respectively. The
195   western margin of Peninsular India, influenced by the Western Ghats, receives heavy rainfall, while the rain
196   shadow region experiences deficient rainfall (Fig. S2.c). The geological and tectonic history, coupled with
197   monsoon climate events, has significantly shaped the present landform (Kale, 2014).

198   The region shown in Fig. 2 is selected as the study area in the Deccan Plateau of Peninsular India. The escarpment
199   of Western Ghats forms the western margin of the Deccan Plateau which serves as the main water divide for the
200   Peninsular River systems. The gentle slope from west to east causes Peninsular rivers such as the Mahanadi,
201   Godavari, Krishna, and Cauvery (Fig. 2) to flow eastwards. Three of these rivers (Godavari, Krishna and Cauvery)
202   originate from the Western Ghats, spread across the area from the Deccan Plateau, flow eastwards, and drain into
203   the Bay of Bengal. The Mahanadi River rises in the mountains of Siwaha bounded by the Eastern Ghats in the
204   south and east, and drain eastwards into the Bay of Bengal. Additional details about the river basins can be found
205   in Text T1 within the Supplementary Information. The study utilizes daily streamflow data (1965-2012) from 62
206   gauges across four river basins, sourced from the Water Resources Information System (WRIS) database. Analysis
207   incorporates a daily gridded rainfall product ($0.25° \times 0.25°$) from the India Meteorological Department (Pai et al.,
208   2014).

209
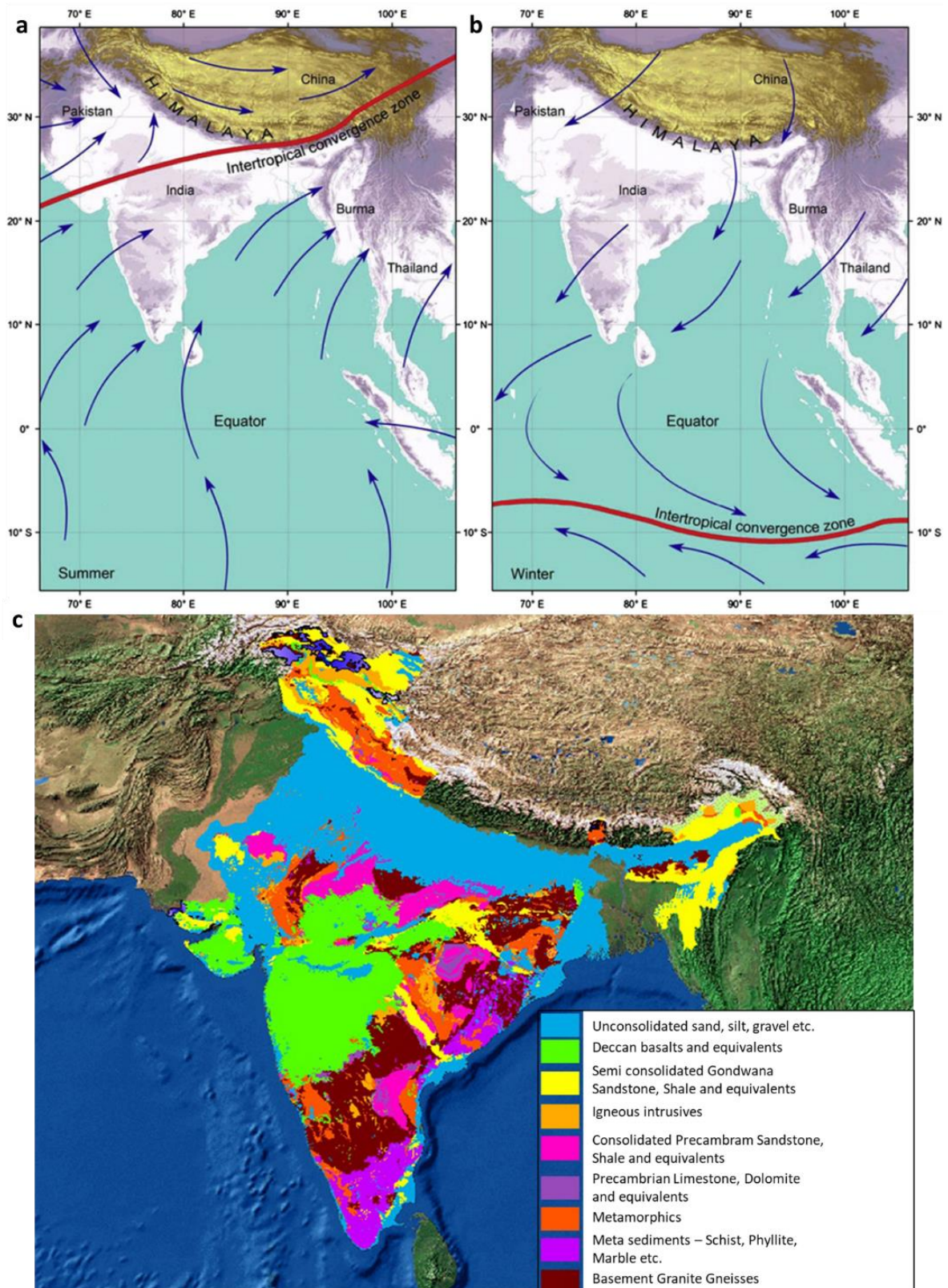
Figure 1. (a) The relation of uplift of Himalaya-Tibetan Plateau and monsoon initiation in India. Monsoon winds blow from the Indian Ocean towards land in the summer (b) during the winter, the Himalaya prevents cold air from passing into the subcontinent and causes the reversal of wind direction and monsoon blow from land toward sea [Reprinted from (Chatterjee et al., 2013)] (c) geology of Peninsular India [Reprinted from: Central Ground Water Board(https://www.aims-cgwb.org/general-background.php)].

215
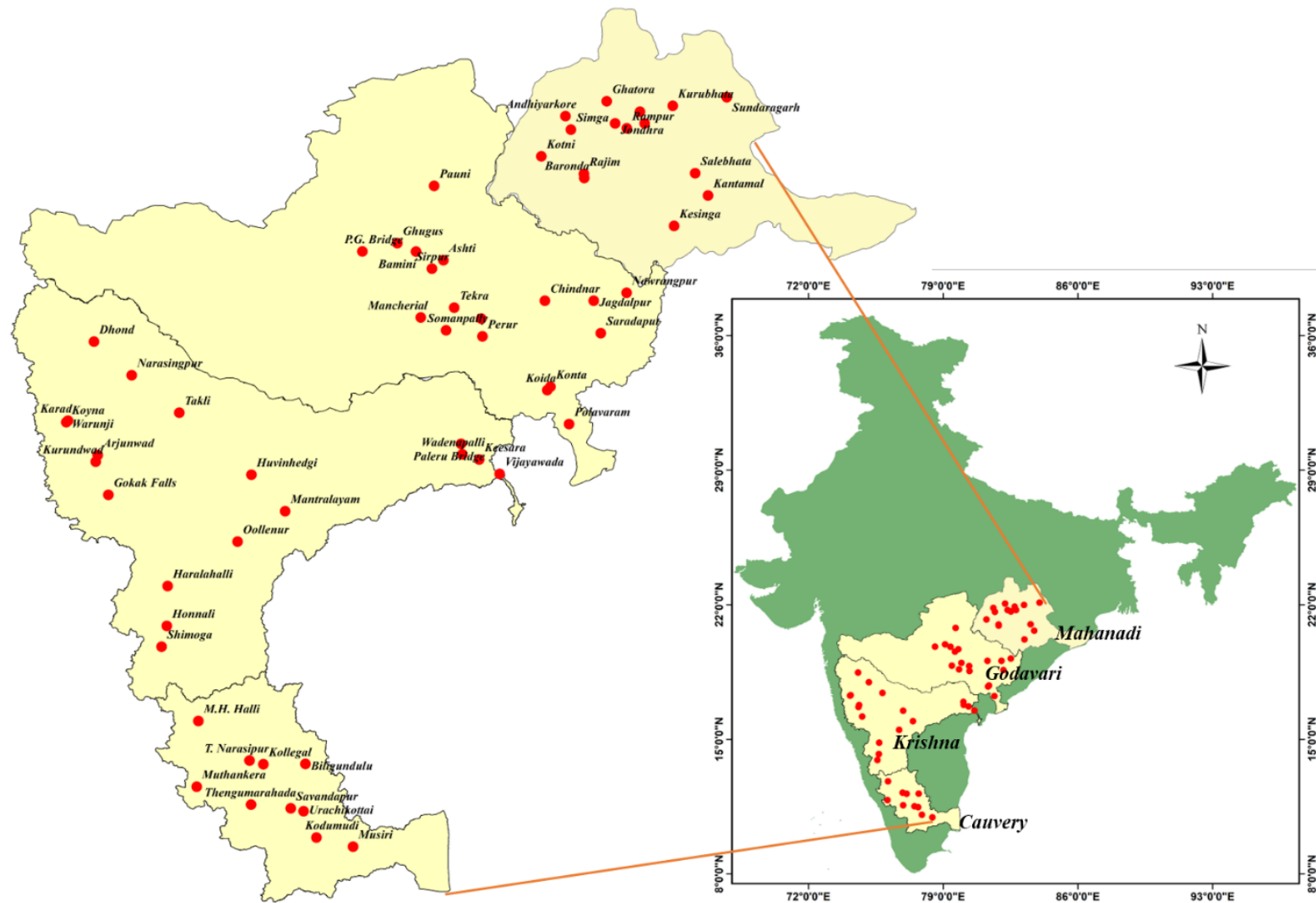
216

217

218   **Figure 2.** Location map of four Peninsular River Basins. Stream gauges considered in this study are marked with red circles.

3 Methodology

Initially, the study employs time scale partitioning to analyse flow duration curves across Peninsular India, focusing on Non-monsoon, South-West monsoon, and North-East monsoon periods in four river basins. The analysis extends to regional scales, encompassing streamflow time series from all gauging stations, and includes process scale partitioning to assess the relative contributions of fast and slow flow components, revealing spatial patterns influenced by climate, geology, and aquifer characteristics.

Additionally, the methodology entails a comprehensive analysis of FDCs for fast and slow flow components across seasons. It includes scaling time series to remove the influence of mean climate and geology, utilizing the statistical distributions to examine parameters influencing FDC shapes. The study explores links between statistical parameters and landscape properties through recession analysis and investigates spatial variation in FDC parameters using descriptors such as latitude, longitude, and catchment area. The final part of the methodology focuses the association between the midsection slope of the FDC and recession parameters, exploring the role of both surface and subsurface processes in controlling the average flow regime of the catchment.

3.1 *Time Scale Partitioning*

The streamflow hydrograph, representing a catchment's response to random rainfall events, is treated as a stochastic time series, with streamflow considered a random variable. Utilizing distribution functions like the cumulative distribution function (CDF) allows for a concise assessment of streamflow variability, aiding in the interpretation and comparison of catchment responses. CDFs have diagnostic and practical value, facilitating the classification of catchments based on flow regimes and supporting probabilistic treatments in engineering design and environmental monitoring. The cumulative distribution function of a random variable (the random variable of interest to us is daily streamflow; Q) expresses the probability that a realization (i.e., observation) of Q does not exceed a specific value q.

The flow duration curve, an equivalent measure of streamflow variability, represents the fraction of time (D) that streamflow is likely to equal or exceed a specified value, expressed mathematically as,

$$D(q) = P[Q \geq q] = 1 - F(q) \tag{1}$$

Despite its probabilistic definition, the flow duration curve is commonly plotted in hydrological applications as q(D), i.e., q (in the vertical axis) as a function of D (in the horizontal axis).

The streamflow time series can be equivalently divided into temporal segments of distinct seasons as well as distinct months. In this case, by joining observed time series over multiple years, FDCs for each time segment can be reconstructed. Assuming independence (as an approximation), these can then be combined to generate annual FDCs. The theory for the time scale partitioning is illustrated in Fig. 3a. The year is divided into three distinct (non-overlapping) seasons, viz. Non-monsoon, South-West, and North-East seasons (for Peninsular India) of

251 relative durations τ_1, τ_2, and τ_3 (with $\tau_1 + \tau_2 + \tau_3 = 1$) respectively. These seasons can be assumed to have
252 distinct characteristics in terms of rainfall variability and how they translate to streamflow variability. The daily
253 streamflow time series is used to construct the seasonal as well as annual FDCs. For example, the FDC of Non-
254 monsoon season is constructed by using the daily streamflow during the period of January – May over the years.
255 Similarly, FDCs for South-West and North-East monsoons are constructed using the daily streamflow during June
256 – September and October – December months over the years respectively and the annual FDC is constructed using
257 daily streamflow values for 365/366 days over the years. The FDCs at monthly time scales are obtained using the
258 daily values of streamflow in a month over the years. The FDCs for the three distinct seasons, i.e., Non-monsoon,
259 South-West monsoon, North-East monsoon, are denoted as $D_{NM}(q)$, $D_{SW}(q)$, and $D_{NE}(q)$ respectively. Initially,
260 the FDCs for each season can be constructed separately (Fig. 3a).

261
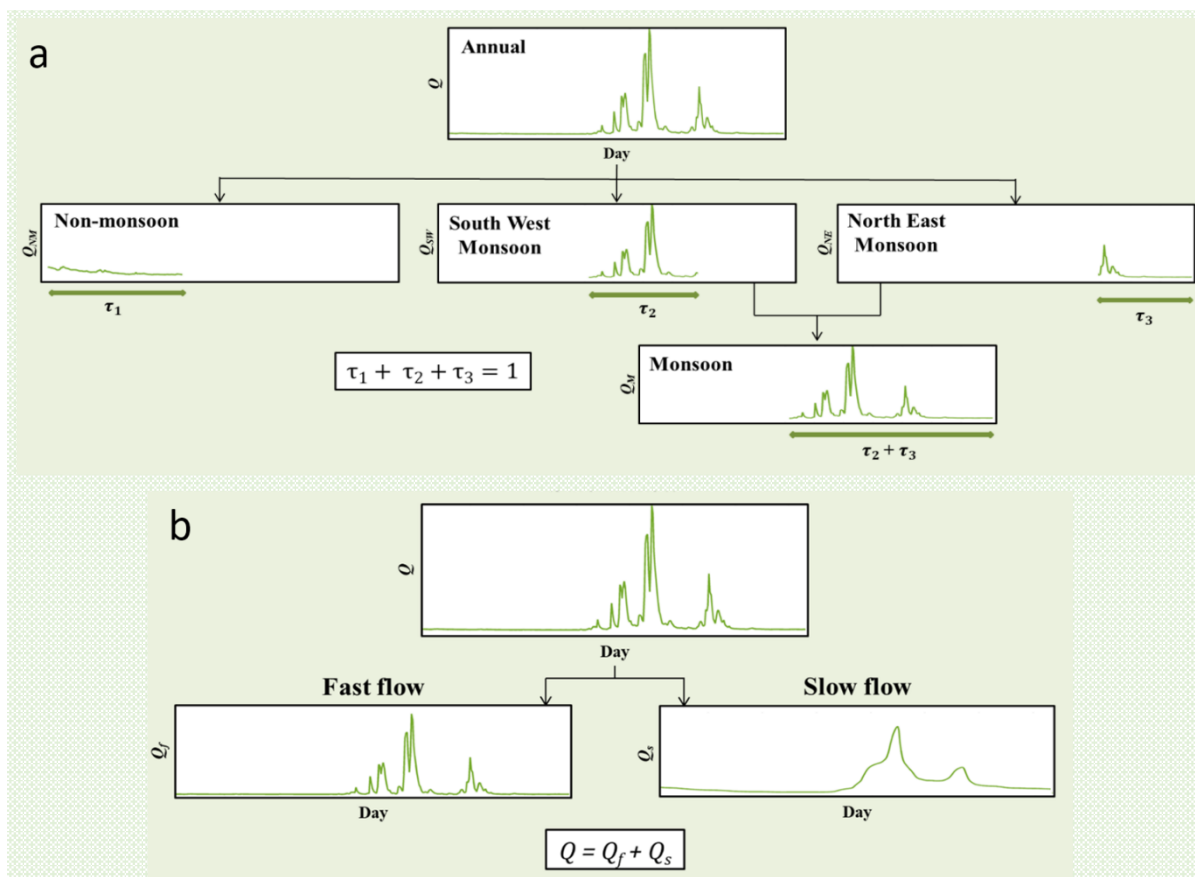
262

263 **Figure 3. Time and process scale partitioning. a)** Scale partitioning into seasonal and monthly time scales. The
264 conceptual framework illustrates the time scale partitioning of streamflow time series into various seasonal
265 components considering patterns of rainfall variability. The annual streamflow time series is decomposed into
266 three components: (1) Non-monsoon flow, (2) South-West monsoon flow, and (3) North-East monsoon flow. **b)**
267 The schematic representation illustrates the process partitioning of streamflow time series into the fast flow and
268 slow flow components.

269 The annual FDC with exceedance probability P $[Q \geq q]$ refers to the probability of flow in annual scale being
270 greater than or equal to q, and is expressed as

$$D(q) = P[Q \geq q] = \tau_1 P_{(NM)}[Q \geq q] + \tau_2 P_{(SW)}[Q \geq q] + \tau_3 P_{(NE)}[Q \geq q] \tag{2}$$

$$\text{or,} \quad D(q) = \tau_1 D_{NM}(q) + \tau_2 D_{SW}(q) + \tau_3 D_{NE}(q) \tag{3}$$

271 where, $P_{(NM)}[Q \geq q]$, $P_{(SW)}[Q \geq q]$ and $P_{(NE)}[Q \geq q]$ refer to, respectively, the probability of flow in Non-
272 monsoon, South-West monsoon and North-East monsoon being greater than q. As the seasons are nonoverlapping

273 the probability of flow being greater than q at annual scale (i.e., P $[Q \geq q]$) can be expressed as the sum of the
274 weighted probabilities of flow being greater than q in the three seasons.

275 In general, the FDC at the annual scale can be constructed as follows:

$$D(q) = \tau_1 D_1(q) + \tau_2 D_2(q) + \cdots + \tau_n D_n(q) \tag{4}$$

276 where n is the number of distinct seasons considered for the analysis and, $\tau_1 + \tau_2 + \cdots + \tau_n = 1$. The validity of
277 the above depends on the assumption that there is no carryover of flows from one season to the next season (which

278 is an approximation). In this study, the assumption of independence between flows across three seasons is checked
279 using multivariate Hoeffding's test (see details in Text T2 of Supplementary Information).

280 The relative contributions of Non-monsoon ($C_{NM \rightarrow AN}$), South-West monsoon ($C_{SW \rightarrow AN}$) and North-East monsoon
281 ($C_{NE \rightarrow AN}$) flows to annual flow can be approximated through following expressions:

$$C_{NM \rightarrow AN} = \frac{\tau_1 E(Q_{NM})}{\tau_1 E(Q_{NM}) + \tau_2 E(Q_{SW}) + \tau_3 E(Q_{NE})} \tag{5}$$

$$C_{SW \rightarrow AN} = \frac{\tau_2 E(Q_{SW})}{\tau_1 E(Q_{NM}) + \tau_2 E(Q_{SW}) + \tau_3 E(Q_{NE})} \tag{6}$$

$$C_{NE \rightarrow AN} = \frac{\tau_3 E(Q_{NE})}{\tau_1 E(Q_{NM}) + \tau_2 E(Q_{SW}) + \tau_3 E(Q_{NE})} \tag{7}$$

282 Similarly, the relative contributions of monthly flows to annual flow can be expressed as:

$$C_{m \rightarrow AN} = \frac{\frac{1}{12} E(Q_m)}{\frac{1}{12} \sum_{m=1}^{12} E(Q_m)} \tag{8}$$

283 Note, as before, these relative contributions to total flow effectively also measure the relative contributions of the
284 seasonal/monthly flows to the mean of the annual flow duration curve.
285 The methodology for constructing annual FDC using seasonal FDC is as follows:

286   1. The empirical PDFs – $f_{NM}(q), f_{SW}(q)$ and $f_{NE}(q)$ are derived for daily streamflow time series for Non-
287   monsoon, South-West monsoon and North-East monsoon seasons respectively.

288   2. These PDFs are then multiplied by scaling factors, τ_1, τ_2 and τ_3 in equation S4. The scaling factors represent
289   relative durations of the three seasons considered. For example, $\tau_1 = 5/12$, as the duration of duration of non-
290   monsoon season is 5 months.

291   3. The PDF of annual flow is estimated as the weighted sum of three scaled density functions corresponding to
292   three seasons (see Eq. S2). The annual flow consists of the daily streamflow for Non-monsoon, South-West
293   monsoon and North-East monsoon seasons.

294   The performance of the time scale partitioning framework is assessed using the metric, root mean square error
295   (RMSE). The method of estimation of q_{sim} is shown in Fig. S3.

296    $$RMSE = \sqrt{\frac{1}{n}\sum_{i=1}^{n}(q_{actual} - q_{sim})^2} \tag{9}$$

297   **3.2 Process Partitioning**

298   Daily streamflow is partitioned in such a way that it approximates the statistical summation of fast flow and slow
299   flow at the daily scale (Fig.3b):

$$Q = Q_f + Q_s \tag{10}$$

300   where Q is the daily streamflow, Q_f is the daily fast flow, Q_s is the daily slow flow.

301   The relative contributions of fast flow ($C_{\to TF}$) and slow flow ($C_{SF \to TF}$) to total flow can be expressed as

$$C_{Q_f \to Q} = \frac{Total\ Fast\ Flow\ Volume}{Total\ Flow\ Volume} \tag{11}$$

$$C_{Q_s \to Q} = \frac{Total\ Slow\ Flow\ Volume}{Total\ Flow\ Volume} \tag{12}$$

302   Note that $C_{Q_f \to Q}$ and $C_{Q_s \to Q}$ effectively measure the relative contributions of fast and slow flows to the mean of
303   the annual flow duration curve.

304   **3.3 Exploring Controls and Spatial Patterns of Flow Duration Curves: Insights from Statistical Distributions
305   and Analysis of Mid-Section Slope**

306   The analysis then extends to the comprehensive analysis of flow duration curves for fast and slow flow
307   components across different seasons, with a focus on understanding their variations and controls. The first step is
308   to scale the fast and slow flow time series by their respective long-term mean values, effectively removing the
309   influence of mean climate and geology. This scaling allows the identification of secondary controls on the shapes
310   of FDCs.

311   The Mixed Gamma Distribution (MGD) is then used to fit the scaled fast and slow flow time series, and the
312   parameters of the MGD are examined for their influence on the FDC shapes (see text T4 of Supplementary

313 Information) Krasovskaia et al., 2006; Botter et al., 2007; Muller and Thompson 2016; Santos et al., 2018. The
314 variation of the parameters of the MGD are explored, regionally and seasonally, considering the influence of mean
315 climate, geology, and complex hydrological processes on fast and slow flows. The performance of the MGD in
316 fitting FDCs is assessed using goodness-of-fit metrics such as the Nash-Sutcliffe efficiency (NSE) and coefficient
317 of determination (R^2). Seasonal variations of MGD parameters are analysed at a regional scale, considering all
318 gauging stations. The study further explores the link between MGD parameters and landscape properties through
319 recession analysis. The studies by Botter et al. (2013), Muller et al. (2014), Basso et al. (2015), Arai et al. (2021),
320 Leong and Yokoo (2022; 2019) collectively enhance understanding of the intricate relationship between recession
321 parameters and FDC characteristics. They emphasize the significant influence of recession parameters on
322 hydrological regimes, catchment-scale attributes, non-linear storage-discharge relations, and the practical
323 applications in predicting FDCs, showcasing a comprehensive exploration of the pivotal role these parameters
324 play in shaping hydrological responses at various spatial scales. Leong and Yokoo (2022) innovative modeling of
325 subsurface components further contribute to a deeper comprehension of the dominant processes influencing FDC
326 shapes. Spatial variation in FDC parameters is then investigated using descriptors such as latitude, longitude, and
327 catchment area.

328 The final aspect of the methodology involves the association between the midsection slope of the FDC and
329 recession parameters, emphasizing the role of both surface and subsurface processes in controlling the average
330 flow regime of the catchment. The methodology aims to unravel the intricate interplay of climate, geology, and
331 hydrological processes in shaping the regional hydrologic signatures of Peninsular India.

4 Results and Discussions

4.1 Time scale partitioning

334 We initially investigated the spatial variations in seasonal and annual flow duration curves across Peninsular India
335 employing the partitioning framework. The annual flow duration curve and seasonal flow duration curves for
336 Non-monsoon, South-West monsoon, and North-East monsoon are shown in Fig. 4 for eight representative
337 gauges, one at the upstream and one at the downstream of each of the four river basins. The estimated annual flow
338 duration curve (red curve) using equation S2 is also shown in Fig. 4. Daily streamflow time series is normalized
339 by catchment area before plotting (on a semi-log paper) the flow duration curve for comparison across the gauging
340 stations. In particular, the annual flow duration curve (black scatter) is reproduced well by the partitioning of both
341 seasonal (red curve in Fig. 4) and monthly flows (red curve in Fig. S4). The mean and variance of annual flows
342 are also reproduced well by the time scale partitioning framework (Fig. S5). This confirms the efficacy of the time
343 scale partitioning approach of seasonal/monthly flows in approximating the annual flow duration curve (see also
344 Fig. S4, Fig. S5.a and Fig. S5.d in Supplementary Material).

345 Another feature that can be observed in Fig. 4 is that in gauging stations located in the northern part of the
346 peninsular region, flow duration curves (FDCs) of South-West monsoon flows (orange curve) are relatively higher
347 than other seasonal FDCs. Given the logarithmic scale used to plot the flows, this dominance is significant. In
348 sites located in the southern part of the region, the dominance of South-West monsoon is not as strong and North-
349 East monsoon flows (blue curve) are also significant.

350 Motivated by these observations, we extracted seasonal and monthly streamflow time series from the entire dataset
351 across all gauging stations to compute the relative contributions of seasonal and monthly flows to the annual flow
352 duration curve. The results are presented in Fig. 5. At the monthly scale (top panel, Fig. 5), the contributions of
353 flows during the months of June to September are much higher than in other months in northern Peninsular basins
354 (Mahanadi and Godavari, Krishna to a less extent). This can be explained by the contribution of monthly rainfall
355 to annual rainfall, which is higher during these months as shown in Fig. S6. On the other hand, in the southernmost
356 Cauvery basin, the dominance of June to September months is relatively not as strong, and there is also a
357 significant contribution during the months of October to December, higher than in northern basins (Fig. 5.d). This
358 can be attributed to the slightly more equal dominance of both South-West (June - September) and North-East
359 (October – December) monsoons over the Cauvery basin (Fig. S6.d) than in the northern basins. This pattern is
360 also reflected at the seasonal scale (bottom panel, Fig. 5), with the contribution of South-West monsoon flow to
361 annual flow being slightly higher than that during the other seasons, and much higher in northern basins. However,
362 the contribution of South-West monsoon to annual flow decreases in southern basins, while the contribution of
363 North-East monsoon increases, as can be seen clearly in Fig. 5.h for the Cauvery basin. The contribution of Non-
364 monsoon to annual flow is also higher in southern basins relative to northern basins. This can be attributed to
365 carry over flows from winter rains during the North-East monsoon, which is more pronounced in the southern
366 part of the region.

367
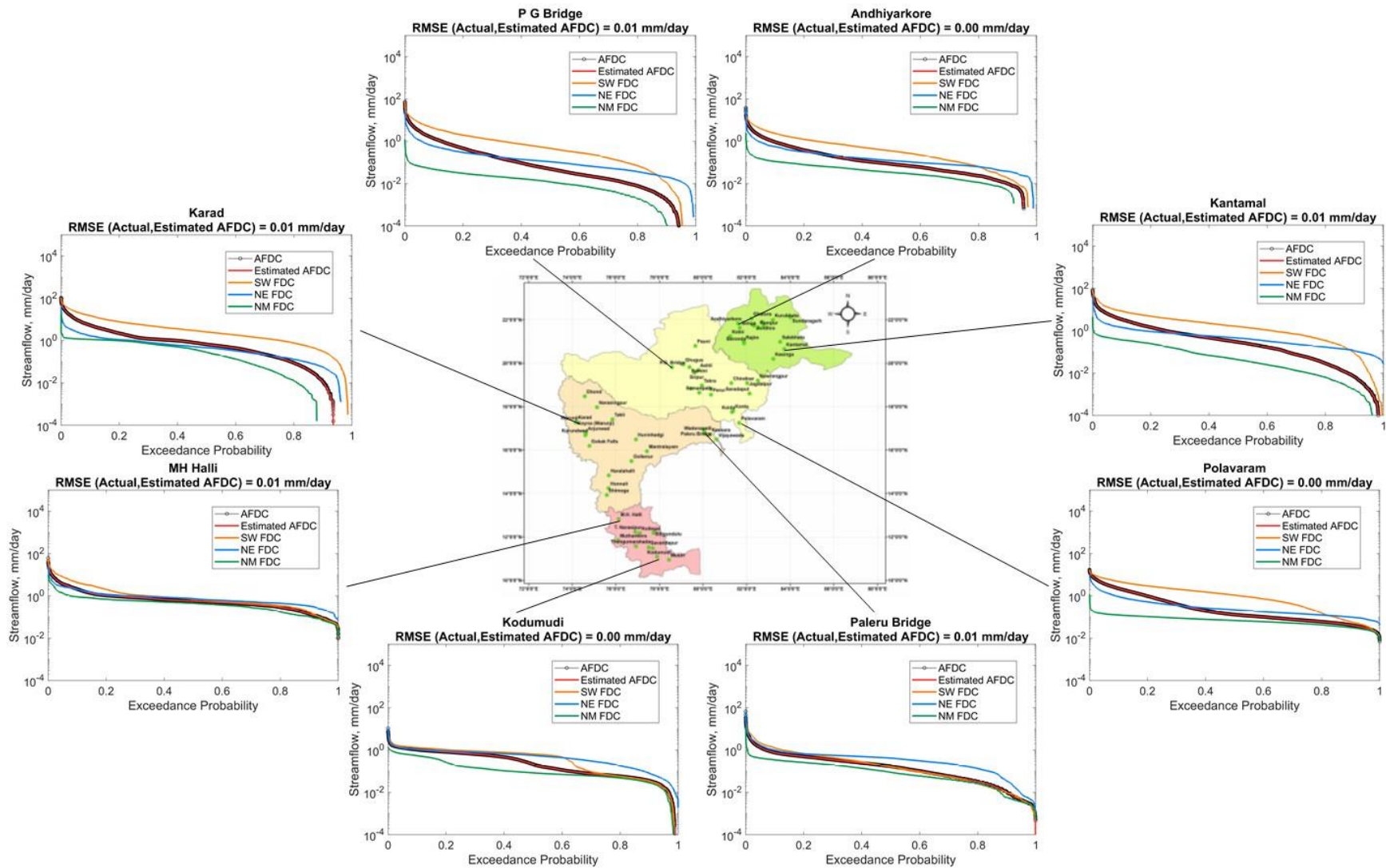
Figure 4. Spatial variations in seasonal and annual flow duration curves across Peninsular India. The time scale partitioning framework of seasonal flows in approximating annual flow duration curves works reasonably well.
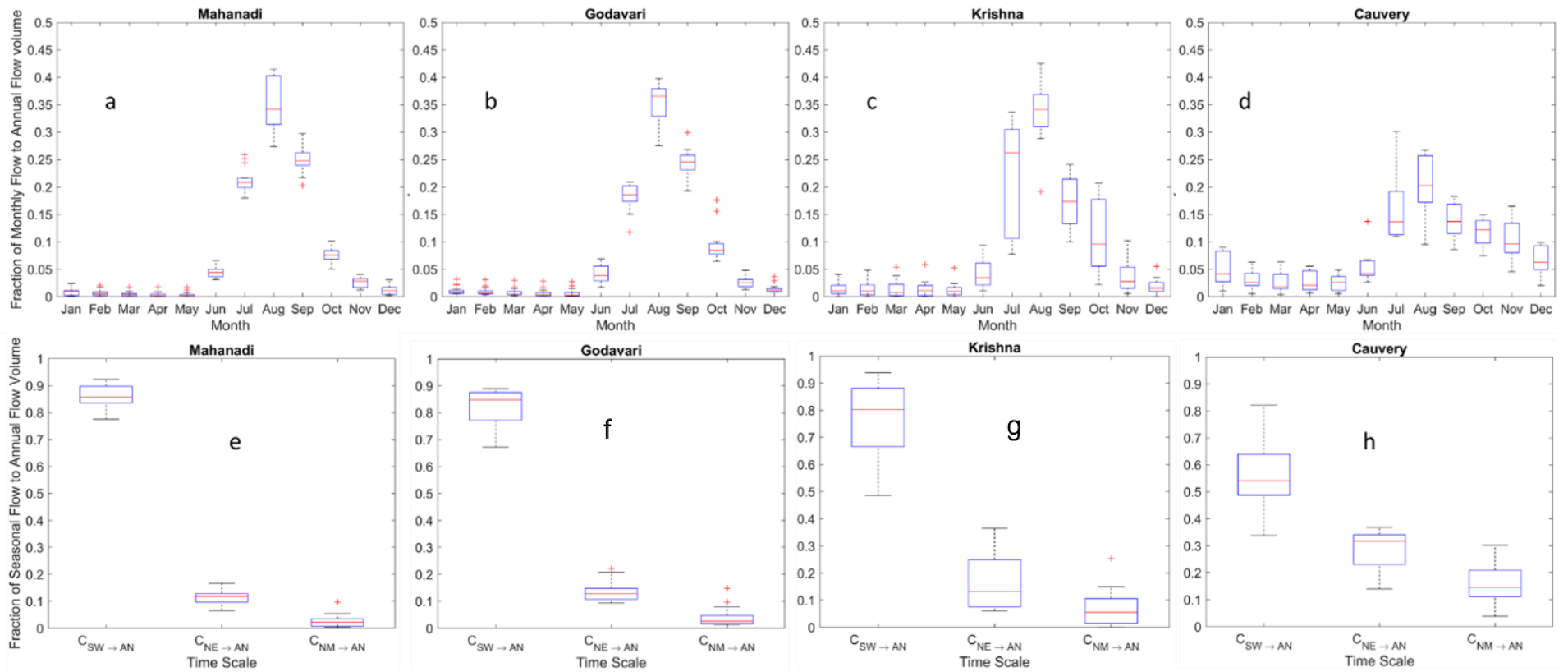
Figure 5. The relative contributions of monthly and seasonal flows to annual flow at basin scale. The contributions of South-West monsoon flow to annual flow increases in northern basins whereas it decreases in southern basins. However, the contributions of North-East monsoon flow to annual flow increases towards southern basins.

373   We next carried out regional scale analysis by considering streamflow time series of all the gauging stations across

374   all four river basins. Similar to basin scale analysis presented before, the relative contributions of seasonal and

375   monthly flows to annual flow are now estimated at the regional scale (Fig. 6). The spatial patterns of South-West

376   and North-East monsoon rainfall across the Peninsular region are plotted for comparison using IMD gridded

377   rainfall product (Fig. 6.b and Fig. 6.e).

378   The contribution of South-West monsoon flows to annual flow increases in the northerly direction (Fig. 6.a). The

379   mountainous region of the southern Peninsula (western part of Krishna basin and north-western part of Cauvery

380   basin) receives high rainfall during the South-West monsoon season (Fig. 6.b – extended till 17° N latitude). The

381   streamflow produced in the headwater regions of southern basins in response to high rainfall, contributes at least

382   70% of the annual flow (Fig. 6.a). Yet, the areal fraction of these high rainfall, headwater regions within the four

383   river basins is quite small and their contributions to the average precipitation or flow at the basin scale is much

384   smaller. There is also considerable variability in the contributions of South-West monsoon flows to annual flow

385   in the sub-basins located at the eastern and south-eastern parts of Krishna and Cauvery basins (represented by the

386   scatter below the regression line till 17° N latitude in Fig. 6.a) due to declining rainfall (Fig. 6c). This considerable

387   variability, on average, reduces the overall contributions of South-West monsoon to annual flow in southern

388   Peninsula with respect to the basins in the northern part.

389   The northern part of the Peninsular region receives comparatively higher rainfall than the southern part without

390   considering the Western Ghats. This increased rainfall is attributed to the movement of low-pressure systems that

391   develop over the Bay of Bengal towards central India (Krishnamurthy & Ajayamohan, 2010; Prakash et al., 2015).

392   The low-pressure systems are a regular feature of South-West monsoon, which brings significant amount of

393   rainfall in the northern part of the Peninsular region (Krishnamurthy & Ajayamohan, 2010). The increased rainfall

394   (Fig. 6.b – after 16° N latitude) is responsible for higher contribution of South-West monsoon flows to annual

395   flow in the northern basins. As the spatial variability of this rainfall is comparatively less than in the southern

396   Peninsular region, there is less variability in the contribution of South-West monsoon flows to annual flow. The

397   spatial variability in South-West monsoon along the south-north direction across Peninsular region can explain

398   the gradient in the contribution of South-West monsoon flows to annual flow in the same direction.

399   On the other hand, the contribution of North-East monsoon flows to annual flow increases in the southerly

400   direction (Fig. 6.d and Fig. 6.e). This can be explained by the fact that the southern part of the Peninsular region

401   receives higher rainfall during North-East monsoon than the rest of the Peninsular region (Fig. 6.f).

402
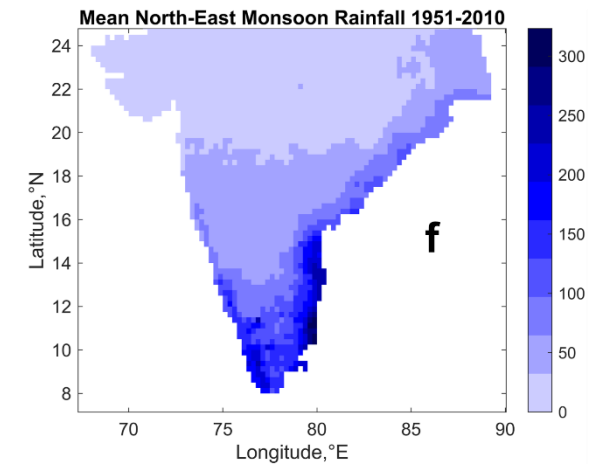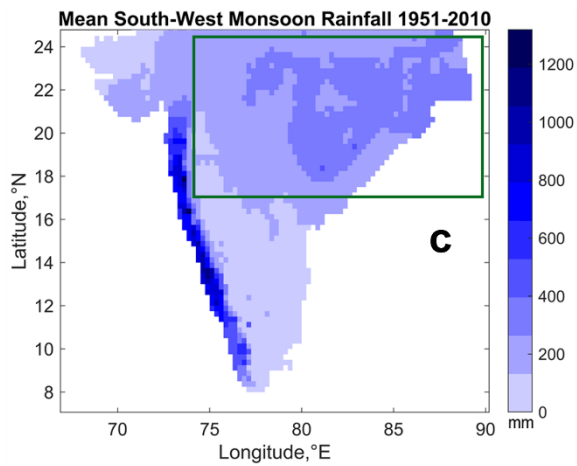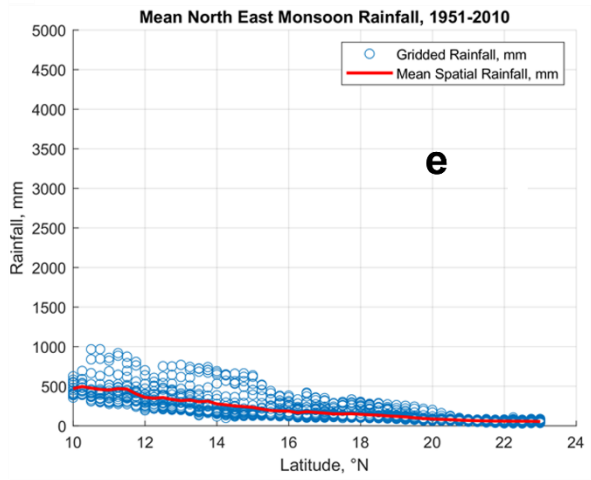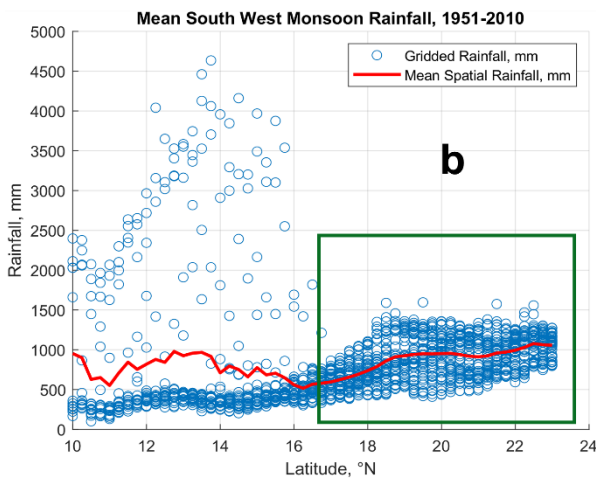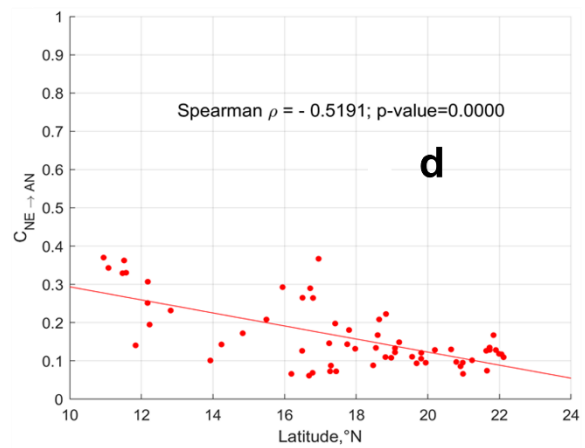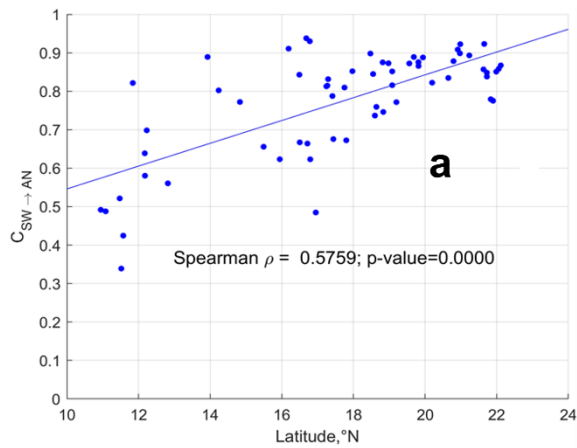
Figure 6. Contribution of seasonal flows to annual flow at regional scale. The spatial variability of South-West and North-East monsoons can explain the variation in contributions of seasonal flows to annual flow across south-north gradient. The green box in (b) indicates the northern part of peninsular region which receives higher rainfall than the southern part. The green box in (c) indicates the spatial extent of the rainfall grids which was considered in figure (b). The red line in figure (b) indicates the mean rainfall – obtained by averaging the rainfall values at a specific latitude (˚N).

The application of the analysis framework used here is based on the critical assumption of independence of flows between different seasons (months), which needs to be critically evaluated. Moisture carry-over across seasons is a confounding issue in the case of strongly seasonal catchments (i.e., exhibiting sharp transition from wet season to dry season in terms of rainfall climatology), specifically when the initial wetness condition at the onset of the dry season depends on the final wetness at the end of wet season and vice-versa. Although most of the rainfall (58-90%) is concentrated during South-West monsoon months (i.e., June – September, red bar in Fig. S7) in Peninsular basins, more than 10% of the annual rainfall is received during North-East monsoon months (i.e., October – December, yellow bar for Cauvery and Krishna in Fig. S7). In addition, more than 8% of annual rainfall occurs in non-monsoon season (i.e., January – May, blue bar in Fig. S7. This highlights that rainfall received during non-monsoon and North-East monsoon seasons are comparable, and thus it is difficult to distinguish the rainfall climatology across these seasons. Therefore, it is challenging to declare these are catchments with seasonally dry climates. In order to justify our assumption in the reconstruction of annual FDC from seasonal flows, we have now conducted a multivariate Hoeffding test (Gaißer et al., 2010) to check the independence between three random variables representing Non-monsoon, South-West Monsoon and North-East Monsoon flows respectively. A value of test statistic – φ^2 – close to zero indicates independence between three random variables. It is observed that except for two stations in Krishna basin, 60 out of 62 stations show independence between flows across the seasons (Fig. S8). This supports appropriateness of the assumption of no carry-over that had been used in this study to construct annual FDC based on seasonal FDCs.

4.2 Combined influence of time scale and process scale partitioning

In order to further explore the climatic and landscape controls of streamflow variability regionally, we next partition streamflow into fast and slow flow components, notionally representing surface runoff, and a combination of subsurface and groundwater flow respectively (Ghotbi et al., 2020a, b). Fast flow is controlled by event scale runoff generation processes and its variability is characterized by topography, land use, soil and rainfall characteristics. On the other hand, climate seasonality and geologic formations of the subsurface are primary controllers of slow flow variability (Ghotbi et al., 2020a, b). The slow flow component is extracted from observed streamflow by using a recursive digital filter (see details in Text T5 of Supplementary Information). The fast flow component is obtained by then subtracting the slow flow from observed streamflow. The relative contributions of fast flow and slow flow to total flow (and hence also mean annual flow) are estimated using equations 11 and 12 respectively, for all the gauging stations across all four basins. The relative contributions of fast and slow flows to total flow at the basin and regional scales (combining all the gauging stations) are shown in Fig. 7. In addition, the long-term mean annual rainfall across the Peninsular region is also presented for comparison and to possibly explain the contributions of fast flow (Fig. 7.h).

The contributions of fast and slow flows to total flow in each of the four river basins is presented in Fig. 7.a to Fig. 7.d, indicating a strong dominance of fast flow in the northern basins (close to 80% in Mahanadi, Godavari and Krishna), and relatively less dominance (around 60%) in the southern Cauvery basin. This dominance of fast flow also shows up at the regional scale (Fig. 7.e). The regional variations of the relative contributions of slow and fast flows to total flow can also be seen in the results for individual gauges presented in Fig. 7.f and Fig. 7.g, respectively. On average, the contribution of slow flow decreases in the northerly direction, while the contribution of fast flow increases in a corresponding way.

The contribution of fast flow to total flow increases in the northern direction of the Peninsular region (Fig. 7.g). The fast flow component of streamflow is generally more responsive to the characteristics of rainfall intensity. The southern part of the region receives high rainfall over Western Ghats along the western edge of Krishna basin and Cauvery basin (Fig. 7.h). In Cauvery basin, the headwater catchments (namely, MH Halli, Muthankera and Thengumarahada in Fig. S6) contribute 57 – 65 % of fast flow to total flow locally. The subbasins located at the western edges of Krishna basin contribute 80% of the fast flow to total flow (between 13° N and 18°N latitudes in Fig. 7.g) locally. However, there is a wide range of variability in the contributions of fast flow to total flow for subbasins located in the eastern part of Krishna basin. The spatial mean rainfall increases and variability decreases after 16° N latitude (Fig. 7.h), which dictate the increased contribution fast flow to total flow. Therefore, the spatial characteristics (mean and variability) of annual rainfall control the south-north gradient in fast flow contributions to total flow. In order to explain the variability in slow flow fraction of total flow, a multivariate regression analysis is performed (details are provided in Text T8). It is observed that the location of the gauges is an important predictor of the slow flow fraction of total flow in Peninsular region, revealing the existence of regional groundwater gradient in the region (Table T1). In addition to the location of the gauges, the recession parameter, β – that controls the aquifer geometry and water level elevation profile during early and late stages of recession – is found to be significant in explaining the slow flow fraction of total flow (Table T1).

The contributions of slow flow to total flow increases in the southerly direction over the Peninsular region (Fig. 7.f). This can be explained by two major factors. Firstly, the Peninsular region is mostly dominated by hard rock geologic formations, where the subsurface flows are controlled by secondary porosities due to weathering and fracturing (Chandra, 2018; Das, 2019). The distribution of these formations is highly heterogenous (Fig. 1.c) and is responsible for baseflow (slow flow) contribution to total flow (Collins et al., 2020; Narasimhan, 2006). For example, 84% of the total area of Cauvery basin is classified as moderate and good groundwater potential zone (Arulbalaji et al., 2019). The influence of such potential regions of Cauvery basin is reflected on the presence of significant amount of slow flow even in the Non-monsoon season (Fig. 8.g and Fig. 8.h). Likewise, 63% of the total area of Krishna basin is classified under same category (Harini et al., 2018). However, the slow flow regime becomes much more seasonal (Fig. 8) in the northern part of the Peninsular region due to limited capability of geologic formations in transmitting slow flow (Patil et al., 2017) as well as strong seasonality in rainfall patterns (Fig. 8). Secondly, the southern part of the Peninsula receives rainfall almost equally during both South-West and North-East monsoons, which is reflected in the bimodal pattern of rainfall seasonality (Fig. 8.g and Fig. 8.h). The compounding effect of bimodal rainfall seasonality and higher fraction of moderate to good groundwater potential zones explains the higher contribution of slow flow to total flow in southern part of the Peninsular region.

479
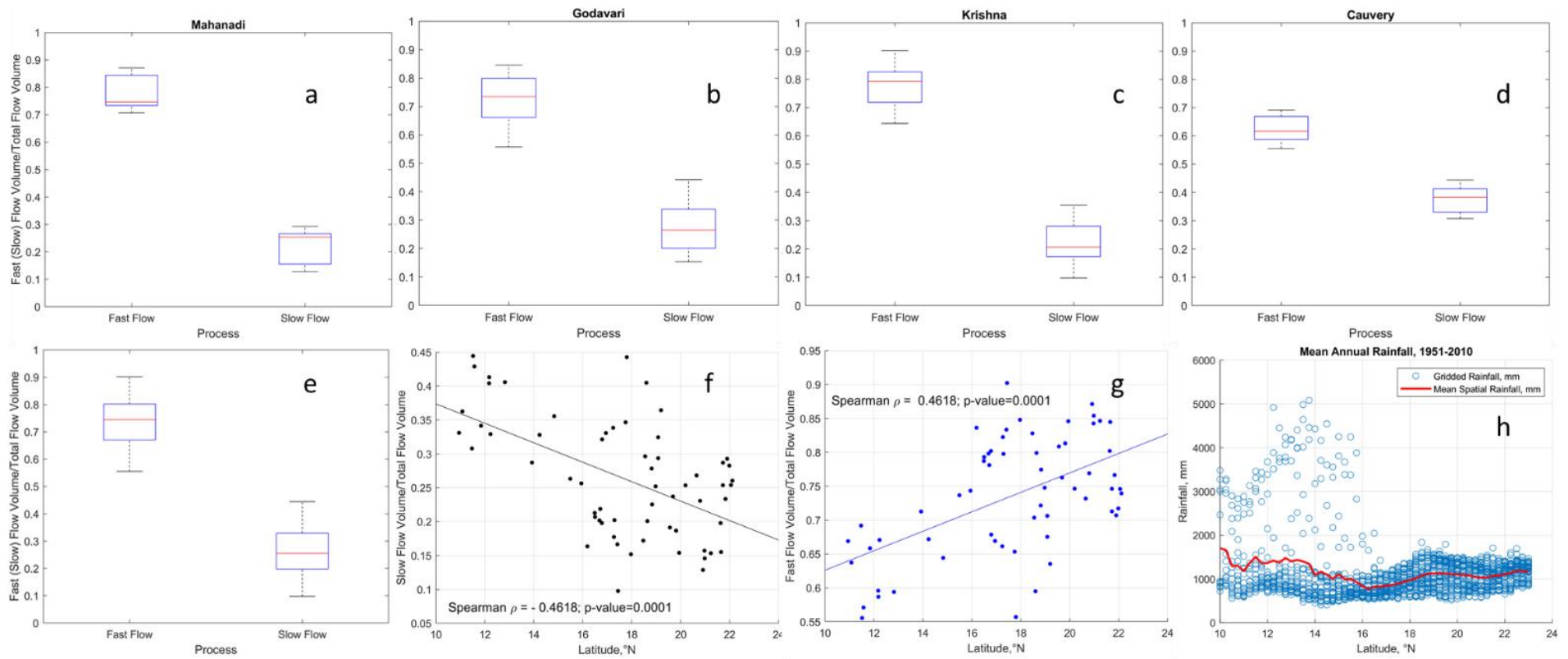
480

481 **Figure 7.** Relative contributions of fast and slow flow to total flow. Consistent higher contribution of fast flow and lower contribution of slow flow to total flow are observed
482 in Peninsular India (a – d) at basin scale. At regional scale, a systematic gradient in fast and slow flow contributions is observed (f and g). The spatial patterns of rainfall (h)
483 can explain the gradient in fast flow contributions. The high scatter of rainfall in the low latitudes represents the heavy rainfall with high variability occurring in the Western
484 Ghats.

485   Further, an investigation of the combined influence of climatic time scales and process time scales is therefore
486   pertinent to fully understand the controls of streamflow variability in this region. To address this question, we
487   extracted the fast and slow flow components for each of the Non-monsoon, South-West monsoon and North-East
488   monsoon seasons. These components are then used to estimate their relative contributions to total flow for the
489   three seasons across all the gauging stations.

490   The relative contributions of fast and slow flow to total flow at basin scale are shown in Fig. 9. It is observed that
491   during the Non-monsoon period, the median contributions of fast and slow flow for Mahanadi, Krishna and
492   Cauvery basins are similar, although there exists considerable variability in their distribution. With the onset of
493   the South-West monsoon, the contribution of fast flow to total flow increases markedly for all the basins, although
494   relatively much less in the Cauvery basin. During the subsequent North-East monsoon season, the contribution of
495   fast flow decreases whereas slow flow contribution increases. The fluctuations in the fast flow contributions can
496   be explained by the onset and withdrawal of the monsoon seasons, which are major contributors to fast flow
497   generation. The fluctuations in the fast flow contributions across seasons can be explained by the differences in
498   the rainfall amount during South-West and North-East monsoons (Fig. 6.c and Fig. 6.f). Among all four basins,
499   the difference in median contributions of fast and slow flow is minimum. These can be attributed to the presence
500   of higher fraction of moderate and good groundwater potential zones (Arulbalaji et al., 2019) which promotes
501   baseflow even in dry periods (Fig. 8.g and Fig. 8.h). The presence of bimodal pattern in rainfall seasonality due
502   to both South-West and North-East monsoons minimizes the difference between the relative contributions of fast
503   and slow flow to total flow.

504
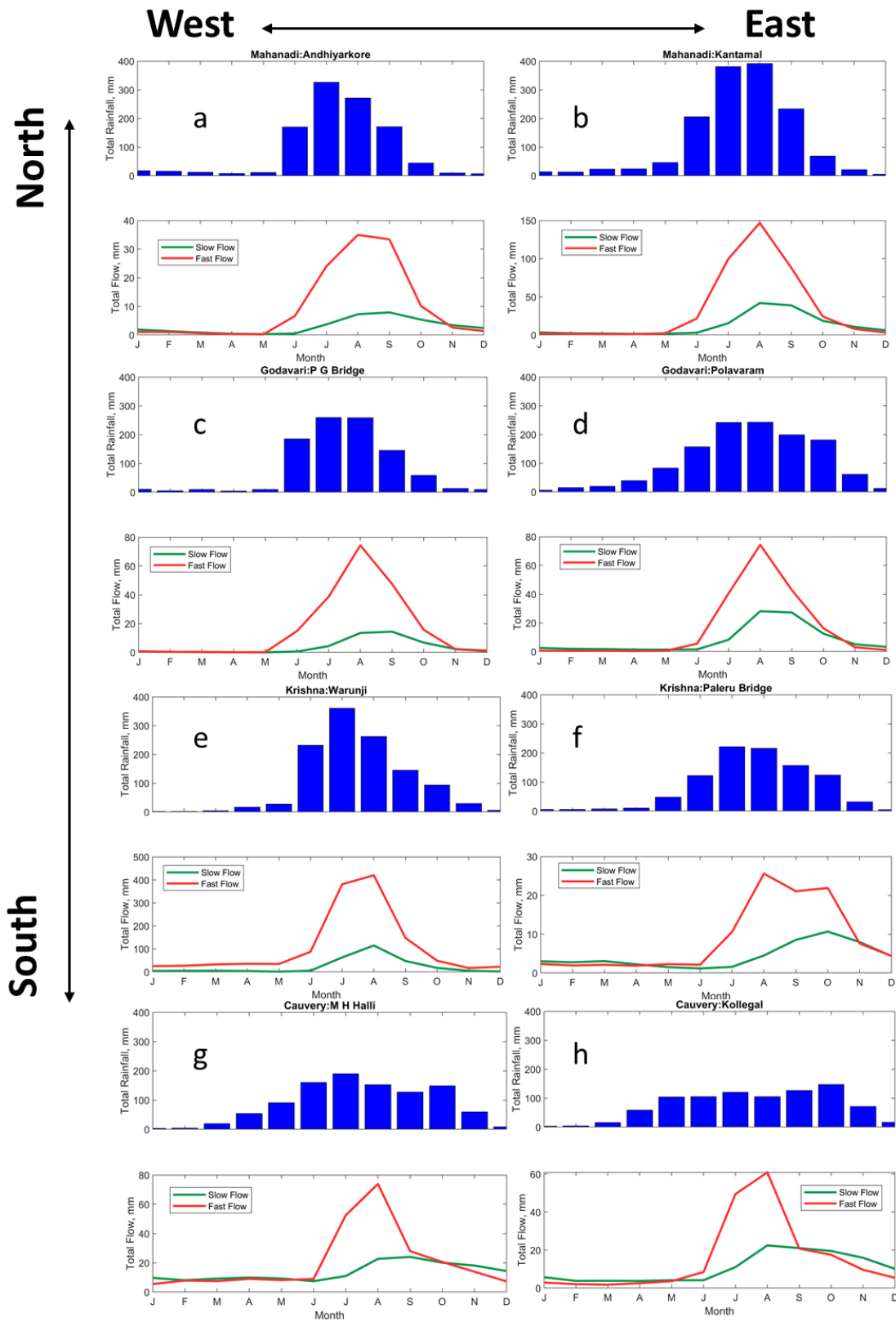
Figure 8. Spatial variation of long-term monthly fast and slow flow components of streamflow at selected gauges in Peninsular region. The blue bar plots represent the long-term monthly rainfall averaged over the sub-basins corresponding to the gauging stations. The seasonality in rainfall patterns changes (unimodal to bimodal) across north-south direction of the Peninsular region.
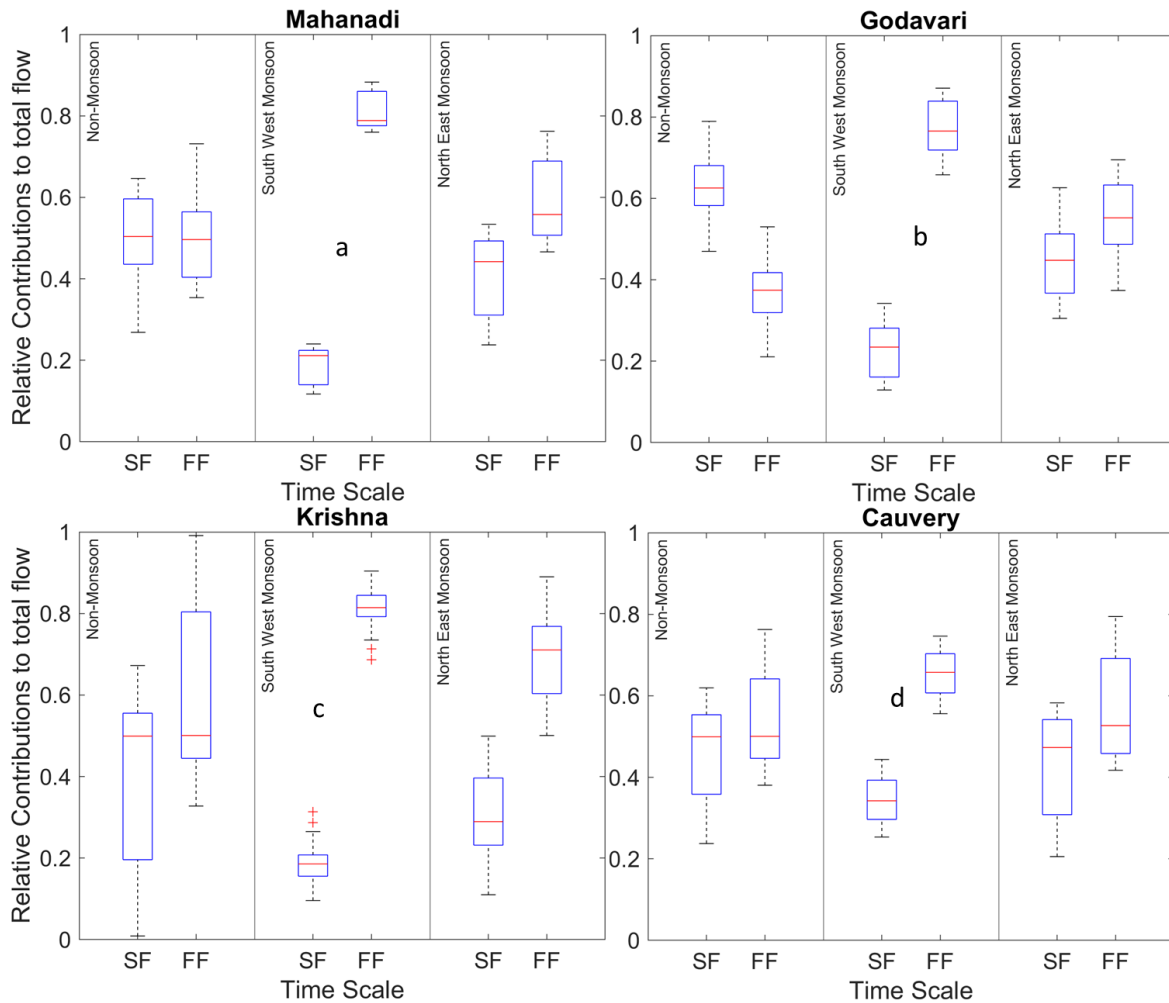
Figure 9. Seasonal contributions of fast (FF) and slow flow (SF) to total flow at basin scale.

5. Stratification of streamflow variability

5.1 Understanding physical controls and spatial variation of flow duration curve by fitting statistical distributions

So far in this paper, in order to understand the physical controls on regional streamflow variability across Peninsular India we have partitioned observed streamflow in two ways: (i) seasonal/monthly flows, and (ii) slow and fast flows. We looked at the relative contributions of these components to mean annual streamflow, looked at how the relative contributions varied regionally, and attributed these to the relative strengths of the monsoons and spatial variations of geological formations. We now return to the FDCs of the flow components, especially the shapes of the FDCs (as reflected in the parameters of the fitted distribution) and look at how they themselves vary regionally.

In our study the fast and slow flow time series are scaled by their respective long-term mean values to remove the influence of mean climate and geology, thus providing an opportunity to identify the secondary controls on the variation of shapes of FDCs. The scaled fast and slow flow time series are now used to fit the mixed gamma distribution (MGD, (see details in Text T4 of Supplementary Information). The parameters of mixed gamma

526 distribution control the shape and orientation of the FDC. For example, the shape parameter k controls the slope
527 of the FDC whereas α controls the zero-flow part of the FDC. However, the parameter θ affects the vertical shift
528 of the FDC. In addition, these parameters are also linked with the mean and variance of the streamflow time series.
529 For example, the scale parameter θ is directly proportional to the mean of the time series whereas, the shape
530 parameter k is inversely proportional to the variance of the time series.

531 As the fast and slow flow time series are scaled with their respective long-term means, the scale parameter (θ) is
532 approximately found to be inversely proportional to shape parameter (k) through the relationship, $k\theta = \frac{1}{1-\alpha}$
533 (Cheng et al., 2012). Therefore, the variations of only k and α – zero-flow probability, are presented in this section.
534 The variation of k can be related to the steepness of the FDC, i.e., smaller values of k will have steeper slopes.

535 The Nash-Sutcliffe efficiency (NSE) and coefficient of determination (R^2) goodness of fit of fast/slow flows to
536 MGD is shown in Fig. S10 (in Supplementary Information). In addition, the observed and simulated fast and slow
537 flow FDCs are compared in Fig. S8 (in Supplementary Information). It is observed that the slow flow component
538 fits well to mixed gamma distribution than fast flow component, as slow flow is most stable component and MGD
539 satisfactorily captured the shape of slow flow FDC. However, MGD adequately captures the shape of fast flow
540 FDCs at upper tail (high flow segment), except for the lower tail (low flow segment). The fast flow processes are
541 governed by more complex processes (for example, infiltration and saturation excess runoff generation, runoff
542 routing, stochastic nature of storm events, properties of soil and topography etc.) than slow flow (for example,
543 climate seasonality and underlying geology of aquifer system).

544 The seasonal variation of parameters of the mixed gamma distribution at regional scale (comprising of all the
545 gauging stations) is presented in Fig. 10. The mixed gamma distribution performed well in fitting the flow duration
546 curves of two flow components across different seasons (Fig. S10). In Fig. 10.a, it is observed that the shape
547 parameter of slow flow is consistently higher than that of fast flow. The shape parameter is inversely proportional
548 to the variance of streamflow. The slow flow exhibits lower variance due to its longer time of residence in the
549 subsurface formations. Moreover, the subsurface formations in Cauvery River basin are more favourable to slow
550 flow in comparison to the other three basins (Fig. 8.g and Fig. 8.h). In addition, the bimodal seasonal pattern of
551 rainfall is also responsible for occurrence of slow flow even in the Non-monsoon period for the southern basins
552 (Fig. 8).

553 The fast flow component exhibits higher variance than the slow flow component. The median shape parameter of
554 fast flow is highest during South-West monsoon season and lowest during North-East monsoon (Fig. 10.a). This
555 can be explained by the lower variance of fast flow during South-West monsoon as the rainfall amount is higher
556 during the season compared to the North-East monsoon (Fig. 6.c and Fig. 6.f). The dominance of both South-
557 West and North-East monsoons in Cauvery basin results in lower variance of fast flow compared to the northern
558 basins. The fast flow duration curves are steeper than the slow flow duration curves for all seasons, as the
559 magnitudes of k for fast flow are smaller than that of slow flow (Fig. 10.a).
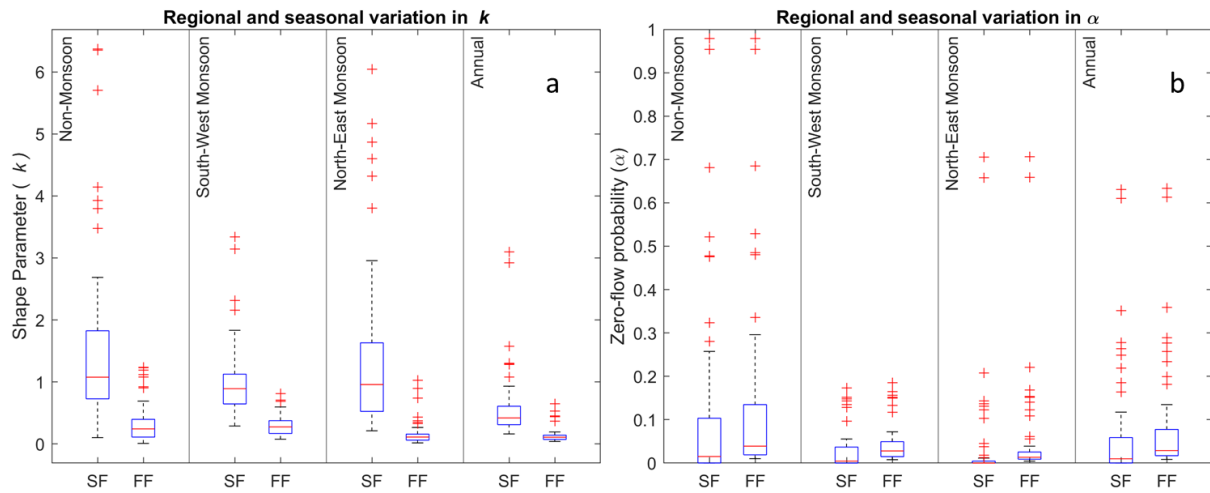
Figure 10. Regional and seasonal variation of k and α parameter of mixed gamma distribution.

The parameter α controls the zero-flow part of the flow duration curve. It is observed that the mean α for slow flow is minimum during South-West monsoon and maximum for Non-monsoon season (Fig. 10.b) on a regional scale. This can be attributed to the combined influence of rainfall during South-West monsoon and the connectivity between underlying geologic formations in the Peninsular region. For the fast flow, the mean α is minimum during the South-West monsoon and maximum during Non-monsoon as the South-West monsoon is the dominating rainfall season in Peninsular India.

The shape parameters (k) of MGD for slow and fast flow components are linked with landscape properties through recession analysis, where the parameters γ and β of power-law relationship are estimated using streamflow data (details in Text T6 in Supplementary Information). It is observed that shape parameter (inversely proportional to variability) of slow flow is positively correlated with β. The parameter β is influenced by aquifer geometry and water table elevation profile defining early and late stages of recession (Tashie et al., 2020a; Tashie et al., 2020b). Higher values of β indicate slow late recessions which is characterized by low variability in slow flow (Fig. 11.a).

The shape parameter of fast flow is negatively correlated with the parameter γ of the power-law relationship (Fig. 11.b). The parameter γ strongly related with the seasonality of catchment wetness and evapotranspiration which are primary governing factors for runoff generation (Dralle et al., 2015; Gnann et al., 2021). In addition, the spatial variation of rainfall also influences the variability of γ (Biswal & Kumar, 2014) which reflects the variability of fast flow.

The variation of the parameters, k and α was also studied using spatial descriptors (latitude and longitude) as explanatory variables to understand the spatial variation of FDCs across south-north, west-east gradients. In addition, the behaviour of these parameters is also assessed using catchment area as another explanatory variable. The regional parameter sets comprising of k and α are next constructed for slow and fast flow processes by including these parameters for all the time series across different gauging stations across the Peninsular region. The Spearman correlation coefficients between these parameters and explanatory variables (i.e., catchment area and spatial descriptors – latitude and longitude) for slow and fast flow processes at seasonal scales are computed.

The schematic representation of significant directions (positive/negative correlations) in Spearman coefficient is shown in Fig. 12.
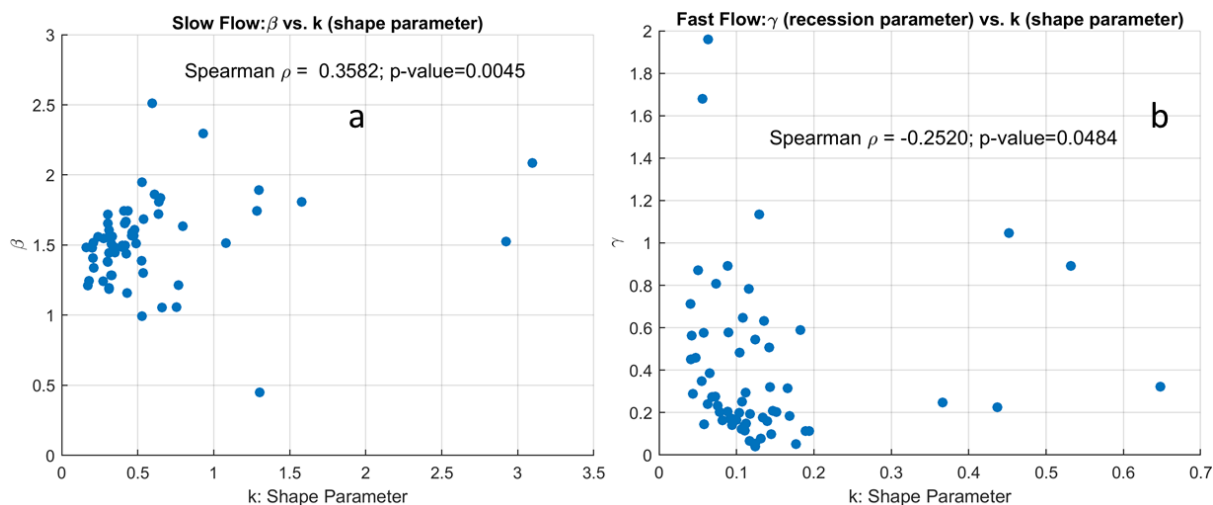
Figure 11. Relationship between flow variability (related inversely to shape parameter, k of mixed gamma distribution) and recession parameters.
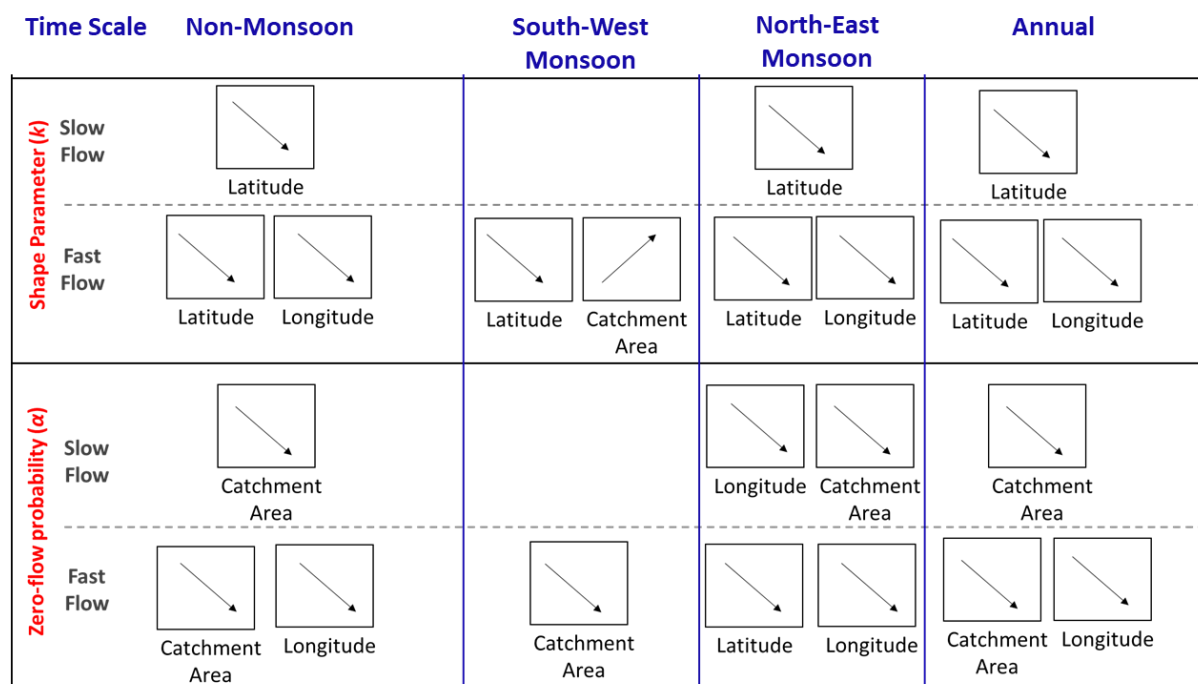
Figure 12. Schematic representation of spatial and temporal variation of parameters of mixed gamma distribution across Peninsular India. The direction of significant Spearman correlation coefficient between model parameters and descriptors (catchment area and spatial descriptors – latitude and longitude) for fast and slow flow across multiple time scale is presented.

The shape parameter of fast flow is found to be positively correlated with catchment area (Fig. 12, top panel), implying lower variability of fast flow in large catchments. This can be attributed to increased smoothening effect of incoming rainfall in larger catchments through various storages, thus reducing the variability of fast flow. Moreover, the shape parameters for fast flow are negatively correlated with spatial descriptors, indicating

increased variability of fast flow along south-north and west-east gradients. This can be partly explained by the bimodal seasonal pattern of rainfall due to dominance of South-West and North-East monsoons, thus reducing the variability of fast flow in the southern part of the region. The rainfall pattern becomes more seasonal (primarily due to South-West monsoon) in the northern part of region which can contribute to increased variability of fast flow. The presence of numerous water retention structures for supporting irrigation in these regions (54 – 75% of Peninsular basins are crop land) can modify the variability of the flow, although we have not analysed this separately in this study.

The shape parameter of slow flow is found to be negatively correlated with latitude, implying that slow flow becomes highly variable in the northern part of the region. This can be explained by the nature of geologic formations in the Cauvery basin that promotes slow flow even during the Non-monsoon period. However, in the northern part of the region, the slow flow tends to become more seasonal and has very limited flow during non-rainy seasons. In addition to the geology, the bimodal seasonal rainfall patterns due to monsoons can play an important role in the variability of slow flow. Apart from the spatial descriptors, the slow flow variability is inversely proportional to catchment area, implying larger catchments have lower slow flow variability than smaller catchments. This can be explained by the proportional increase in area of contribution to slow flow with increase in catchment size, thus reducing the variability in slow flow for larger catchments.

The parameter α is found to be negatively correlated with catchment area (Fig. 12, bottom panel) for fast and slow processes, implying zero-flow probabilities are lower for larger catchments. The higher residence time of water in larger catchment due to various kinds of storages facilitates flow in river even in Non-monsoon season, thus reducing the zero-flow probabilities. In addition, the parameter α of both slow and fast flow are negatively correlated with longitude, implying lower zero-flow probabilities along west-east direction. This can be attributed to natural declining elevation (Fig. S1.b) which promotes both fast and slow flow towards eastern direction.

5.2 Understanding physical controls and spatial variation of seasonal flow duration curve using mid-section slope

Apart from mean, variance and no-flow frequency, the midsection slope of the FDC – estimated using $\frac{\ln(Q_{33p}) - \ln(Q_{66p})}{0.66 - 0.33}$, where Q_{33p} and Q_{66p} represent the streamflow values at 33rd and 66th percentiles respectively – is connected to the average flow regime of the catchment, which is controlled by both surface and subsurface processes (Yokoo & Sivapalan, 2011; Chouaib et al., 2018). The association of the slope of FDC with the parameters pertaining to recession analysis is presented in Fig. 13.

629

630
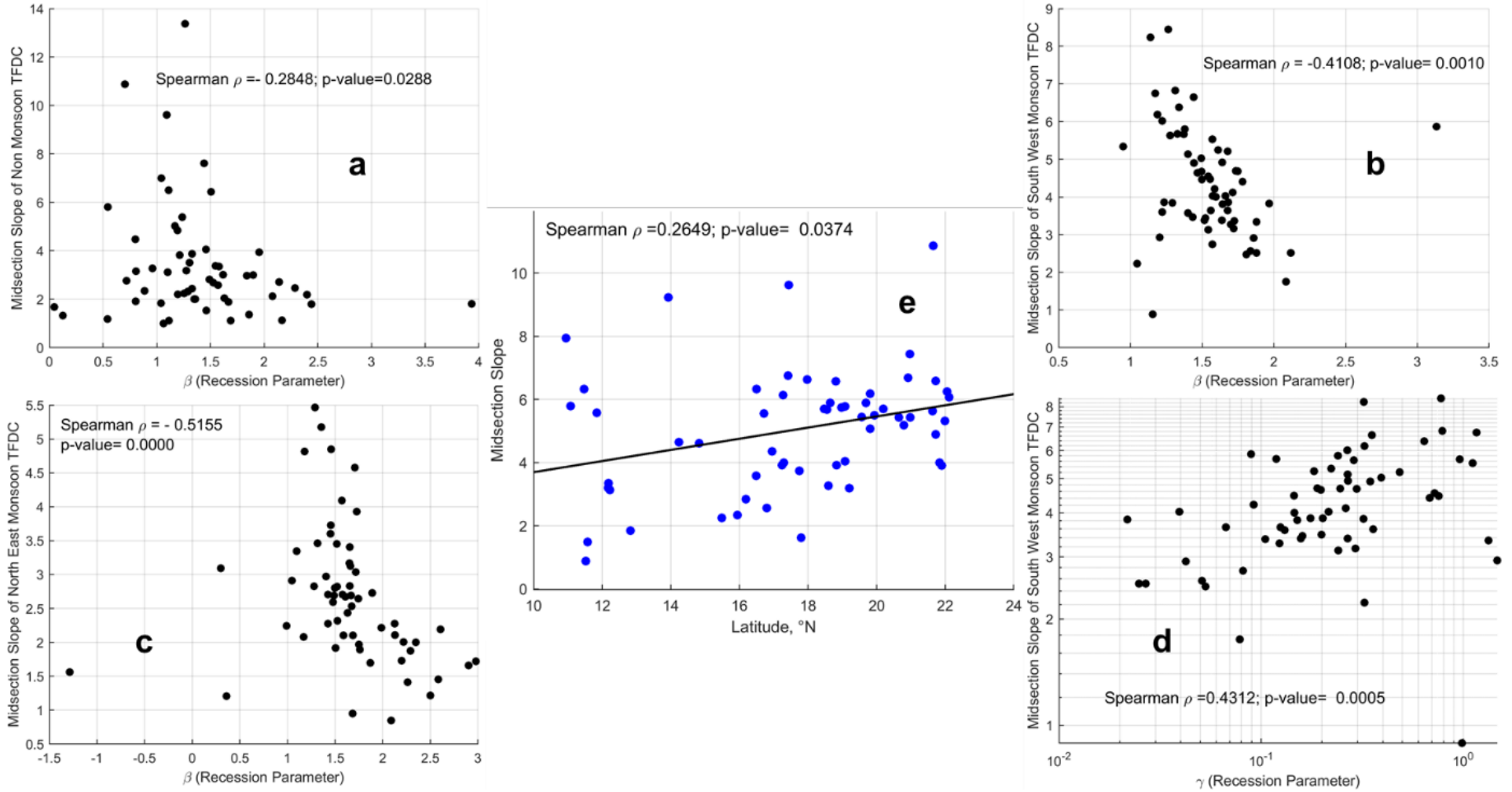
631   **Figure 13.** Association between streamflow variability and recession parameters.

During Non-monsoon and North East monsoon seasons (Fig. 13a and Fig. 13c) – when rainfall is comparatively less than South West monsoon – a significant association between flow variability and β highlights the importance of slow flow and recession characteristics controlled by aquifer geometry and water table elevation profile. In addition to significant association with β during South West monsoon (Fig. 13b), the midsection slope of FDC is positively correlated with γ – the parameter which is strongly related with the seasonality of catchment wetness, evapotranspiration and spatial variation in rainfall – revealing the importance of land surface processes in variability of streamflow variability.

A coherent pattern in variability of streamflow (via. Midsection slope of FDC) is observed across South – North gradient of the Peninsular region (Fig. 13e). This systematic pattern in streamflow variability reflects the influence of combined functioning of subsurface and land surface processes on regional hydrologic signatures of Peninsular India.

6. Conclusions

The comprehensive analysis of spatial variations in seasonal and annual flow duration curves across Peninsular India has provided valuable insights into the controls of streamflow variability at different scales. The partitioning framework employed in this study effectively approximated annual flow duration curves, confirming its efficacy in capturing the intricate dynamics of seasonal and monthly flows. Noteworthy spatial patterns emerged, with gauging stations in the northern part of the peninsula exhibiting higher dominance of South-West monsoon flows in contrast to the more balanced contributions observed in the southern regions, where North-East monsoon flows also played a significant role.

The regional-scale analysis unveiled the influence of spatial patterns of monsoon rainfall, showing increased contributions of South-West monsoon flows in the northerly direction and elevated contributions of North-East monsoon flows in the southerly direction. The study also delved into the partitioning of streamflow into fast and slow components, revealing a dominance of fast flow in northern basins and an increasing contribution of slow flow in the southerly direction. Factors such as rainfall intensity, geologic formations, and groundwater gradients were identified as critical controls shaping these flow characteristics. The investigation of combined influences of climatic time scales and process time scales further enriched our understanding of streamflow variability. Seasonal fluctuations in fast and slow flow contributions highlighted the dynamic nature of streamflow response to monsoon onset and withdrawal. The study emphasized the importance of considering both climatic and landscape factors across different scales to comprehensively grasp the controls of streamflow variability in the Peninsular region.

By undertaking an extensive analysis of flow duration curves for both fast and slow flow components across different seasons, the study aims to understand the variations and controls governing these hydrological patterns. The initial step of scaling the fast and slow flow time series by their respective long-term mean values serves as a crucial tool in isolating secondary controls on FDC shapes, effectively removing the influence of mean climate and geology. The subsequent use of the Mixed Gamma Distribution to fit the scaled time series allows for an advanced examination of the parameters influencing FDC shapes, with a focus on the key factors of shape parameter (k) and probability of zero flows (α). The seasonal variations of MGD parameters at a regional scale

reveal the impact of monsoons on streamflow characteristics. Notably, the consistently higher shape parameters for slow flow highlight the lower variance attributed to longer residence times in subsurface formations, emphasizing the influence of geological features.

Further exploration into the relationships between MGD parameters and landscape properties through recession analysis enhances our understanding of hydrological controls. The positive correlation between the shape parameter of slow flow and recession parameter β, influenced by aquifer geometry, contrasts with the negative correlation between the shape parameter of fast flow and the parameter γ, associated with seasonality of catchment wetness and evapotranspiration. Spatial variation analysis using descriptors like latitude, longitude, and catchment area unveils significant correlations, offering insights into the influence of geographical factors on FDC shapes. The correlation of fast flow shape parameters with catchment area suggests reduced variability in larger catchments, while the negative correlation of slow flow shape parameters with latitude indicates increased variability in the northern part of the region. The examination of zero-flow probabilities controlled by the parameter α reveals noteworthy trends. Larger catchments exhibit lower zero-flow probabilities, and the negative correlation of α with longitude highlights the spatial influence along the west-east direction. Finally, the study explores the midsection slope of the FDC, connecting it to average flow regimes controlled by both surface and subsurface processes. Associations with recession analysis parameters underline the integrated influence of aquifer geometry and land surface processes on streamflow variability across Peninsular India.

In summary, the methodology employed in this study offers a systematic and insightful approach to unravelling the complexities of streamflow variability across Peninsular India. This study not only enhances our understanding of the relative contributions and shapes of FDCs but also sheds light on the intricate interplay of geological, spatial, and hydrological factors influencing streamflow variability in this region.

We acknowledge, however, that in recent times streamflow variability in Peninsular India has been significantly impacted by anthropogenic activities, including significant land use and land cover changes, and other human interferences such as the building of dams and the extraction of water from both rivers and from groundwater aquifers for human use. The present study has not explored the effects of human impacts: their impacts on both temporal (inter-decadal) and spatial (regional) variations of the FDCs is left for future work. Further work is also needed to understand in more detail the causes and the relative contributions of regional patterns precipitation and geological formations on streamflow partitioning.

On the methodological front, there is opportunity to refine the analysis used here to incorporate the statistical cross-correlation between fast and slow flows in the reconstruction of the FDC for total streamflow, by adopting generalized approaches (e.g., copulas). In the exploration of the relative contributions of the monsoons, there is scope to extend the analysis framework to partition the streamflow variability guided by the actual breakdown into the seasons each year in a more flexible way, as opposed to the static way. This is likely to make the results of the analysis more robust and less uncertain. Finally, in the process domain, the filter-based separation of total streamflow into fast and slow flow can be variably impacted by catchment size, introducing some uncertainty into the partitioning of the FDC of total streamflow into its fast flow and slow flow components. Future work in this area should explore ways to overcome these methodological shortcomings.

707 *Data availability*. The streamflow datasets used for the analysis are accessible from
708 https://indiawris.gov.in/wris/#/. The daily India Meteorological Department (IMD) gridded rainfall product at
709 spatial resolution of 0.25° × 0.25°
710 (https://www.imdpune.gov.in/Clim_Pred_LRF_New/Grided_Data_Download.html) from Pai et al., (2014) is
711 used. The function baseflow, used for partitioning total flow to slow flow is downloaded from
712 https://in.mathworks.com/matlabcentral/fileexchange/58525-baseflow-filter-using-the-recursive-digital-filter-
713 technique.

714 *Author contributions*. PD, JM, and MS conceptualized the work, developed the methodology, and carried out the
715 data curation, formal analysis, validation, and writing of the original draft. MS and PPM reviewed the initial
716 manuscript, and PPM provided the resources needed for this work.
717 *Competing interests*. The authors declare that they have no conflict of interest.

718 *Acknowledgements*. PD acknowledges DST INSPIRE Faculty Fellowship (DST/INSPIRE/04/2022/001952
719 Faculty Reference No.: IFA22-EAS 114) received from Department of Science and Technology, Government of
720 India, in Earth and Atmospheric Sciences Division of 2022 call. MS acknowledges the award of a Satish Dhawan
721 Endowed Visiting Professorship that enabled him to visit the Interdisciplinary Centre for Water Research
722 (ICWaR) at the Indian Institute of Science, which allowed him to participate in the research activity that
723 culminated in this paper. MS also acknowledges the generous support and facilities provided by ICWaR that made
724 his stay a very productive one.

725

726 **References**

727 Arai, R., Toyoda, Y., & Kazama, S. (2021). Runoff recession features in an analytical probabilistic streamflow
728 model. Journal of Hydrology, 597, 125745.

729 Arnold, J. G. and Allen, P. M.: Automated methods for estimating baseflow and ground water recharge from
730 streamflow records, J. Am. Water Resour. Assoc., 35, 411–424, https://doi.org/10.1111/j.1752-
731 1688.1999.tb03599.x, 1999.

732 Arnold, J. G., Allen, P. M., Muttiah, R., and Bernhardt, G.: Automated Base Flow Separation and Recession
733 Analysis Techniques, Ground Water, 33, 1010–1018, https://doi.org/10.1111/j.1745-6584.1995.tb00046.x, 1995.

734 Arulbalaji, P., Sreelash, K., Maya, K., and Padmalal, D.: Hydrological assessment of groundwater potential zones
735 of Cauvery River Basin, India: a geospatial approach, Environ. Earth Sci., 78, 1–21,
736 https://doi.org/10.1007/s12665-019-8673-6, 2019.

737 Basso, S. and Botter, G.: Streamflow variability and optimal capacity of run-of-river hydropower plants, Water
738 Resour. Res., 48, 1–13, https://doi.org/10.1029/2012WR012017, 2012.

739 Basso, S., Schirmer, M., & Botter, G. (2015). On the emergence of heavy-tailed streamflow distributions.
740 Advances in Water Resources, 82, 98-105.

741 Bhardwaj, K., Shah, D., Aadhar, S., and Mishra, V.: Propagation of Meteorological to Hydrological Droughts in
742 India, J. Geophys. Res. Atmos., 125, https://doi.org/10.1029/2020JD033455, 2020.

743 Biswal, B. and Nagesh Kumar, D.: Study of dynamic behaviour of recession curves, Hydrol. Process., 28, 784–
744 792, https://doi.org/10.1002/hyp.9604, 2014.

745 Blum, A. G., Archfield, S. A., Vogel, R. M., and Survey, G.: On the probability distribution of daily streamflow
746 in the United States, Hydrol. Earth Syst. Sci., 21, 3093–3103, https://doi.org/https://doi.org/10.5194/hess-21-
747 3093-2017, 2017.

748 Botter, G., Zanardo, S., Porporato, A., Rodriguez-Iturbe, I., and Rinaldo, A.: Ecohydrological model of flow
749 duration curves and annual minima, Water Resour. Res., 44, 1–12, https://doi.org/10.1029/2008WR006814, 2008.

750 Botter, G., Basso, S., Rodriguez-Iturbe, I., & Rinaldo, A. (2013). Resilience of river flow regimes. Proceedings
751 of the National Academy of Sciences, 110(32), 12925-12930.

752 Carlier, C., Wirth, S. B., Cochand, F., Hunkeler, D., & Brunner, P. (2018). Geology controls streamflow dynamics.

Journal of Hydrology, 566, 756-769.

Chanapathi, T. and Thatikonda, S.: Investigating the impact of climate and land-use land cover changes on hydrological predictions over the Krishna river basin under present and future scenarios, Sci. Total Environ., 721, 137736, https://doi.org/10.1016/j.scitotenv.2020.137736, 2020.

Chandra, P. C.: Groundwater of Hard Rock Aquifers of India, 61–84, https://doi.org/10.1007/978-981-10-3889-1_5, 2018.

Chatterjee, S., Scotese, C. R., and Bajpai, S.: The Restless Indian plate and its epic voyage from Gondwana to Asia: Its tectonic, paleoclimatic, and paleobiogeographic evolution, Spec. Pap. Geol. Soc. Am., 529, 1–147, https://doi.org/10.1130/2017.2529, 2017.

Cheng, L., Yaeger, M., Viglione, A., Coopersmith, E., Ye, S., and Sivapalan, M.: Exploring the physical controls of regional patterns of flow duration curves – Part 1: Insights from statistical analyses, Hydrol. Earth Syst. Sci., 16, 4435–4446, https://doi.org/10.5194/hess-16-4435-2012, 2012.

Chouaib, W., Caldwell, P. V., and Alila, Y.: Regional variation of flow duration curves in the eastern United States: Process-based analyses of the interaction between climate and landscape properties, J. Hydrol., 559, 327–346, https://doi.org/10.1016/j.jhydrol.2018.01.037, 2018.

Collins, L. S., Loveless, S. E., Muddu, S., Buvaneshwari, S., Palamakumbura, R. N., Krabbendam, M., Lapworth, D. J., Jackson, C. R., Gooddy, D. C., Nara, S. N. V., Chattopadhyay, S., and MacDonald, A. M.: Groundwater connectivity of a sheared gneiss aquifer in the Cauvery River basin, India, Hydrogeol. J., 28, 1371–1388, https://doi.org/10.1007/s10040-020-02140-y, 2020.

Costa, V. and Fernandes, W.: Regional Modeling of Long-Term and Annual Flow Duration Curves: Reliability for Information Transfer with Evolutionary Polynomial Regression, J. Hydrol. Eng., 26, 1–12, https://doi.org/10.1061/(asce)he.1943-5584.0002051, 2021.

Das, S.: Frontiers of Hard Rock Hydrogeology in India, in: Ground Water Development - Issues and Sustainable Solutions, Springer Singapore, Singapore, 35–68, https://doi.org/10.1007/978-981-13-1771-2_3, 2019.

Deshpande, N. R., Kothawale, D. R., and Kulkarni, A.: Changes in climate extremes over major river basins of India, Int. J. Climatol., 36, 4548–4559, https://doi.org/10.1002/joc.4651, 2016.

Dralle, D., Karst, N., and Thompson, S. E.: a, b careful: The challenge of scale invariance for comparative analyses in power law models of the streamflow recession, Geophys. Res. Lett., 42, 9285–9293, https://doi.org/10.1002/2015GL066007, 2015.

Durighetto, N., Mariotto, V., Zanetti, F., McGuire, K. J., Mendicino, G., Senatore, A., & Botter, G. (2022). Probabilistic description of streamflow and active length regimes in rivers. Water Resources Research, 58, e2021WR031344. https:// doi.org/10.1029/2021WR031344

Gadgil, S.: The Indian Monsoon and Its Variability, Annu. Rev. Earth Planet. Sci., 31, 429–467, https://doi.org/10.1146/annurev.earth.31.100901.141251, 2003.

Fenicia, F., Kavetski, D., Savenije, H. H., Clark, M. P., Schoups, G., Pfister, L., & Freer, J. (2014). Catchment properties, function, and conceptual model representation: is there a correspondence? Hydrological Processes, 28(4), 2451-2467.

Ghotbi, S., Wang, D., Singh, A., Blöschl, G., and Sivapalan, M.: A New Framework for Exploring Process Controls of Flow Duration Curves, Water Resour. Res., 56, https://doi.org/10.1029/2019WR026083, 2020a.

Ghotbi, S., Wang, D., Singh, A., Mayo, T., and Sivapalan, M.: Climate and Landscape Controls of Regional Patterns of Flow Duration Curves Across the Continental United States: Statistical Approach, Water Resour. Res., 56, https://doi.org/10.1029/2020WR028041, 2020b.

Gnann, S. J., McMillan, H. K., Woods, R. A., and Howden, N. J. K.: Including Regional Knowledge Improves Baseflow Signature Predictions in Large Sample Hydrology, Water Resour. Res., 57, https://doi.org/10.1029/2020WR028354, 2021.

Gupta, H., Reddy, K. K., Gandla, V., Paridula, L., Chiluka, M., and Vashisth, B.: Freshwater discharge from the large and coastal peninsular rivers of India: A reassessment for sustainable water management, Environ. Sci. Pollut. Res., 29, 14400–14417, https://doi.org/10.1007/s11356-021-16811-0, 2022.

801 Harini, P., Sahadevan, D. K., Das, I. C., Manikyamba, C., Durgaprasad, M., and Nandan, M. J.: Regional
802 Groundwater Assessment of Krishna River Basin Using Integrated GIS Approach, J. Indian Soc. Remote Sens.,
803 46, 1365–1377, https://doi.org/10.1007/s12524-018-0780-4, 2018.

804 Harman, C. and Troch, P. A.: What makes Darwinian hydrology "Darwinian"? Asking a different kind of question
805 about landscapes, Hydrol. Earth Syst. Sci., 18, 417–433, https://doi.org/10.5194/hess-18-417-2014, 2014.

806 Kale, V. S., Hire, P., and Baker, V. R.: Flood Hydrology and Geomorphology of Monsoon-dominated Rivers:
807 The Indian Peninsula, Water Int., 22, 259–265, https://doi.org/10.1080/02508069708686717, 1997.

808 Kale, V. S., Vaidyanadhan, R.: Landscapes and Landforms of India, edited by: Kale, V. S., Springer Netherlands,
809 Dordrecht, 105–113 pp., https://doi.org/10.1007/978-94-017-8029-2_6, 2014.

810 Koneti, S., Sunkara, S. L., and Roy, P. S.: Hydrological modeling with respect to impact of land-use and land-
811 cover change on the runoff dynamics in Godavari river basin using the HEC-HMS model, ISPRS Int. J. Geo-
812 Information, 7, https://doi.org/10.3390/ijgi7060206, 2018.

813 Krishnamurthy, V. and Ajayamohan, R. S.: Composite Structure of Monsoon Low Pressure Systems and Its
814 Relation to Indian Rainfall, J. Clim., 23, 4285–4305, https://doi.org/10.1175/2010JCLI2953.1, 2010.

815 Kumar Raju, B. C. and Nandagiri, L.: Analysis of historical trends in hydrometeorological variables in the upper
816 Cauvery Basin, Karnataka, India, Curr. Sci., 112, 577–587, https://doi.org/10.18520/cs/v112/i03/577-587, 2017.

817 Krasovskaia, I., Gottschalk, L., Leblois, E., & Pacheco, A. (2006). Regionalization of flow duration curves.
818 Climate variability and change: hydrological impacts, 105-110.

819 Leong, C., & Yokoo, Y. (2019). An interpretation of the relationship between dominant rainfall-runoff processes
820 and the shape of flow duration curve by using data-based modeling approach. Hydrological Research Letters,
821 13(4), 62-68.

822 Leong, C., & Yokoo, Y. (2022). A multiple hydrograph separation technique for identifying
823 hydrological model structures and an interpretation of dominant process controls on flow
824 duration curves. *Hydrological Processes*, 36(4), e14569. https://doi.org/10.1002/hyp.14569

825 Magilligan, F. J. and Nislow, K. H.: Changes in hydrologic regime by dams, Geomorphology, 71, 61–78,
826 https://doi.org/10.1016/j.geomorph.2004.08.017, 2005.

827 Magilligan, F. J., Nislow, K. H., and Graber, B. E.: Scale-independent assessment of discharge reduction and
828 riparian disconnectivity following flow regulation by dams, Geology, 31, 569, https://doi.org/10.1130/0091-
829 7613(2003)031<0569:SAODRA>2.0.CO;2, 2003.

830 Milliman JD, F. K.: River discharge to the coastal ocean: a global synthesis, river discharge to the coastal ocean:
831 a global synthesis, Cambridge University Press, 2011.

832 Müller, M. F., & Thompson, S. E. (2016). Comparing statistical and process-based flow duration curve models in
833 ungauged basins and changing rain regimes. Hydrology and Earth System Sciences, 20(2), 669-683.

834 Narasimhan, T. N.: Ground Water in Hard-Rock Areas of Peninsular India: Challenges of Utilization, Ground
835 Water, 44, 130–133, https://doi.org/10.1111/j.1745-6584.2005.00167.x, 2006.

836 Nathan, R. J. and McMahon, T. A.: Evaluation of automated techniques for base flow and recession analyses,
837 Water Resour. Res., 26, 1465–1473, https://doi.org/10.1029/WR026i007p01465, 1990.

838 Pai, D. S., Sridhar, L., Rajeevan, M., Sreejith, O. P., Satbhai, N. S., and Mukhopadhyay, B.: Development of a
839 new high spatial resolution (0.25° × 0.25°) long period (1901-2010) daily gridded rainfall data set over India and
840 its comparison with existing data sets over the region, Mausam, 1, 1–18, 2014.

841 Patil, S., Kulkarni, H., Bhave, N., Development, W. R., Forum, P., Dialogue, P., and Conflicts, W.: Groundwater
842 in the Mahanadi River Basin, https://doi.org/10.13140/RG.2.2.11561.95846, 2017.

843 Prakash, S., Mitra, A. K., and Pai, D. S.: Comparing two high-resolution gauge-adjusted multisatellite rainfall
844 products over India for the southwest monsoon period, Meteorol. Appl., 22, 679–688,
845 https://doi.org/10.1002/met.1502, 2015.

846 Rajeevan, M., Unnikrishnan, C. K., Bhate, J., Niranjan Kumar, K., and Sreekala, P. P.: Northeast monsoon over

847   India: variability and prediction, Meteorol. Appl., 19, 226–236, https://doi.org/10.1002/met.1322, 2012.

848   Ramachandra, T. V: Global Biodiversity Hotspot - Western Ghats : Water Tower of Peninsular India and Precious
849   Heritage for Posterity, 2018.

850   Rao, P. G., Chanapathi, T., Thatikonda, S., Koneti, S., Sunkara, S. L., Roy, P. S., Kumar Raju, B. C., and
851   Nandagiri, L.: Investigating the impact of climate and land-use land cover changes on hydrological predictions
852   over the Krishna river basin under present and future scenarios, Curr. Sci., 7, 577–587,
853   https://doi.org/10.18520/cs/v112/i03/577-587, 2017.

854   Rehana, S. and Mujumdar, P. P.: River water quality response under hypothetical climate change scenarios in
855   Tunga-Bhadra river, India, Hydrol. Process., 25, 3373–3386, https://doi.org/10.1002/hyp.8057, 2011.

856   Rehana, S. and Mujumdar, P. P.: Climate change induced risk in water quality control problems, J. Hydrol., 444–
857   445, 63–77, https://doi.org/10.1016/j.jhydrol.2012.03.042, 2012.

858   Richards, F. D., Hoggard, M. J., and White, N. J.: Cenozoic epeirogeny of the Indian peninsula, Geochemistry,
859   Geophys. Geosystems, 17, 4920–4954, https://doi.org/10.1002/2016GC006545, 2016.

860   Saha, K. R., Mooley, D. A., and Saha, S.: The Indian monsoon and its economic impact, GeoJournal, 3,
861   https://doi.org/10.1007/BF00257706, 1979.

862   Santos, A. C., Portela, M. M., Rinaldo, A., & Schaefli, B. (2018). Analytical flow duration curves for summer
863   streamflow in Switzerland. Hydrology and earth system sciences, 22(4), 2377-2389.

864   Searcy, J. K.: Flowduration curves, Man. Hydrol. U.S. Geol. Surv., 1959.

865   Sinha, J., Sharma, A., Khan, M., and Goyal, M. K.: Assessment of the impacts of climatic variability and
866   anthropogenic stress on hydrologic resilience to warming shifts in Peninsular India, Sci. Rep., 8, 13833,
867   https://doi.org/10.1038/s41598-018-32091-0, 2018.

868   Sivapalan, M.: From engineering hydrology to Earth system science: milestones in the transformation of
869   hydrologic science, Hydrol. Earth Syst. Sci., 22, 1665–1693, https://doi.org/10.5194/hess-22-1665-2018, 2018.

870   Smakhtin, V. U.: Smakhtin 2010- Low flow hydrology.pdf, J. Hydrol. Hydrol., 240, 147–186,
871   https://doi.org/10.1016/S0022-1694(00)00340-1, 2001.

872   Sreelash, K., Mathew, M. M., Nisha, N., Arulbalaji, P., Bindu, A. G., and Sharma, R. K.: Changes in the
873   hydrological characteristics of Cauvery river draining the eastern side of southern Western Ghats, India, Int. J.
874   River Basin Manag., 18, 153–166, https://doi.org/10.1080/15715124.2020.1719119, 2020.

875   Stewart, M. K. (2015). Promising new baseflow separation and recession analysis methods
876   applied to streamflow at Glendhu Catchment, New Zealand. *Hydrology and Earth System*
877   *Sciences*, *19*(6), 2587-2603.

878   Tashie, A., Pavelsky, T., and Band, L. E.: An Empirical Reevaluation of Streamflow Recession Analysis at the
879   Continental Scale, Water Resour. Res., 56, https://doi.org/10.1029/2019WR025448, 2020a.

880   Tashie, A., Pavelsky, T., and Emanuel, R. E.: Spatial and Temporal Patterns in Baseflow Recession in the
881   Continental United States, Water Resour. Res., 56, https://doi.org/10.1029/2019WR026425, 2020b.

882   Tongal, H., Demirel, M. C., and Moradkhani, H.: Analysis of dam-induced cyclic patterns on river flow dynamics,
883   Hydrol. Sci. J., 62, 626–641, https://doi.org/10.1080/02626667.2016.1252841, 2017.

884   Vogel, R. M. and Fennessey, N. M.: Flow-Duration Curves. I: New Interpretation and Confidence Intervals, J.
885   Water Resour. Plan. Manag., 120, 485–504, https://doi.org/10.1061/(ASCE)0733-9496(1994)120:4(485), 1994.

886   Vogel, R. M. and Fennessey, N. M.: Flow Duration Curves Ii: a Review of Applications in Water Resources
887   Planning, JAWRA J. Am. Water Resour. Assoc., 31, 1029–1039, https://doi.org/10.1111/j.1752-
888   1688.1995.tb03419.x, 1995.

889   Wagener, T., Blöschl, G., Goodrich, D. C., Gupta, H. V., Sivapalan, M., Tachikawa, Y., Troch, P. A., and Weiler,
890   M.: A synthesis framework for runoff prediction in ungauged basins, in: Runoff Prediction in Ungauged Basins,
891   Cambridge University Press, 11–28, https://doi.org/10.1017/CBO9781139235761.005, 2013.

892   Ye, S., Yaeger, M., Coopersmith, E., Cheng, L., & Sivapalan, M. (2012). Exploring the physical controls of

893 regional patterns of flow duration curves–Part 2: Role of seasonality, the regime curve, and associated process
894 controls. Hydrology and Earth System Sciences, 16(11), 4447-4465.

895 Yokoo, Y. and Sivapalan, M.: Towards reconstruction of the flow duration curve: Development of a conceptual
896 framework with a physical basis, Hydrol. Earth Syst. Sci., 15, 2805–2819, https://doi.org/10.5194/hess-15-2805-
897 2011, 2011.

898